The Abdus Salam
International Centre for Theoretical Physics

United Nations
Educational, Scientific
and Cultural Organization

International Atomic
Energy Agency

H4.SMR/1775-42

"8th Workshop on Three-Dimensional Modelling of
Seismic Waves Generation, Propagation and their Inversion"

25 September - 7 October 2006

Q and its Variation in the Earth's Crust and Upper Mantle

Brian J. Mitchell

Department of Earth and Atmospheric Sciences
Saint Louis University
U.S.A.

Q and its Variation in the Earth's Crust and Upper Mantle

Brian J. Mitchell
Department of Earth and Atmosperic Sciences
Saint Louis University

October 1, 2006

1 INTRODUCTION

Seismic waves have long been known to attenuate at a rate greater than that predicted by geometrical spreading of their wave fronts. L. Knopoff pointed out more than four decades ago (Knopoff, 1964) that much of that attenuation must occur because of intrinsic anelastic properties of the Earth. Were it not for that fortunate circumstance, waves generated by all past earthquakes, as noted by Knopoff, would still be reverberating in the Earth today. Scattering, since it redistributes rather than absorbs wave energy, would not accomplish the same thing.

Practical aspects of seismic wave attenuation include the need to take it into consideration when determining earthquake magnitudes and to include its effect when computing realistic synthetic seismograms. In addition, seismologists must know the attenuation structure in the Earth if they wish to determine dispersion that is produced by anelasticity (Jeffreys, 1967; Liu et al., 1976). The principle of causality requires that such velocity dispersion accompany intrinsic attenuation (Lomnitz, 1957; Futterman, 1962; Strick, 1967).

A commonly used measure of the efficiency of wave propagation is the quality factor Q or its inverse, the internal friction Q^{-1}. The latter quantity has most often been defined by the expression

$$Q^{-1} = \Delta E / 2\pi E_{max} \qquad (1)$$

where ΔE is the energy lost per cycle and E_{max} is the maximum elastic energy contained in a cycle. O'Connell and Budiansky (1978) proposed replacing maximum energy by average stored energy in equation 1, a change that requires the integer 4 replace 2 in that equation. That form of the definition permits writing Q as the ratio of the real to imaginary part of the complex elastic modulus.

Determinations available in the 1960's from seismic observations and laboratory measurements suggested that Q was independent of frequency (Knopoff, 1964). That conclusion, however, conflicted with the frequency dependences known for single relaxation mechanisms that exhibit relatively narrowly peaked spectra for Q^{-1} centered at a characteristic frequency. Liu et al. (1976) reconciled those two observations by considering that Q^{-1} over the seismic frequency band in the Earth consists of a superposition of many relaxation mechanisms for which maxima occurred at different frequencies. That superposition produces a continuous absorption band with a nearly frequency-independent Q^{-1} distribution in the seismic frequency band (Figure 1).

A later model (Anderson and Given, 1982) constructed to explain variations of Q for various depths in the Earth proposed that Q^{-1} varies with frequency as ω^{+1} at the higher end of the absorption band, as ω^{-1} at the lower end and ω^{α} in the central portion (Anderson and Given, 1982). They found that a single absorption band with minimum $Q = 80$, $\alpha = 0.15$ and a width of five decades centered at different frequencies for different depths in the mantle could satisfy many of the known values of Q in the early 1980's.

At crustal depths the frequency dependence of Q is usually described in the equation $Q = Q_o f^{\zeta}$ where Q_o is a reference frequency and ζ is the frequency depen-

dence parameter. For shear-wave Q (Q_μ) it appears to be between about 0.0 and 1.0 and varies regionally, with depth in the crust, and with frequency.

The following sections present a review of what has been learned about seismic wave attenuation from earliest studies to the present. It is a rapidly growing field for which measurements have only recently become sufficiently plentiful and reliable to allow mapping at relatively small scales. It has long been known that measurement errors are large and it has recently become clear that systematic, rather than random, errors are the greatest cause of concern in Q determinations.

We will begin by briefly reviewing many of the early studies of Q. We follow this by considering portions of the Earth that still must be considered to be one-dimensional in its distribution of Q. This includes the entire Earth below the upper mantle. Finally we present methodologies for determining Q and what is known about its regional variation, separately considering the crust and upper mantle.

2 EARLY STUDIES

Although seismic wave attenuation did not become a popular area of research until the 1970's, the first contributions appeared not long after global deployments of seismographs in the early 1900's. Here we describe several important studies completed before 1970. Those studies, in addition to providing the first estimates of Q for several phases, provided the first inklings of the difficulties associated with amplitude measurements.

G.H. Angenheister, working in Göttingen, Germany in 1906, reported the first known measurements of the attenuation rate of a seismic wave. Instruments at that time were still primitive and surface waves consequently dominated most seismograms recorded by Göttingen's Wiechert seismometers. Angenheister (1906) used records from those instruments to measure the amplitude decay of 20-s surface waves for three different segments of the same great-circle path and found the decay rate to be about 0.00025/km. For group velocities near 3 km/s that rate corresponds to a Q value of about 200, a value that lies within the range of commonly measured 20-s attenuation coefficient values today. He later published what was probably the first report of regional variations of surface-wave attenuation (Angenheister, 1921) in which he found that the decay of surface-wave amplitudes along oceanic paths was greater than that along continental paths. We now know that this result holds only for those cases where attenuation over relatively low-Q oceanic paths is compared to attenuation over high-Q continental paths (Mitchell, 1995).

B. Gutenberg also made some early determinations of Q using surface waves. He determined a Q value of 70 for Love waves at 100-s period (Gutenberg, 1924), and a value of 200 for Rayleigh waves at 20-s period (Gutenberg, 1945a). The latter value corresponds well with Angenheister's earlier measurement of Rayleigh-wave attenuation at that period. Gutenberg also determined Q for body phases, first finding a Q of 1300 for 4-s P and PKP waves (Gutenberg, 1945b). He then measured Q for three body-wave phases at different periods (Gutenberg, 1958) finding a Q's of 2500 for P and PP at 2 s, and 400 for P and PP at 12 s. In the same study he also measured Q for S waves finding values of 700 at 12 s and 400 at 24 s. Press (1956) also determned Q for S waves finding it to by 500 or less.

Evernden (1955) studied the arrival directions of SV-, Rayleigh- and Love-wave phases using a tripartite array in California and found that all of those phases deviated from great-circle paths between the events and the array. Although Evernden did not address Q he brought attention to the fact that seismic waves may deviate from a great-circle path during propagation, a problem that continues, to this day, to plague determinations of Q from amplitude measurements.

The 1960's produced the first definitive evidence for lateral variations of body-wave Q even over relatively small distances. Asada and Takano (1963), in a study of the predominant periods of teleseismic phases recorded in Japan, found that those periods differed at two closely spaced stations and attributed that to differences in crustal Q. Ichikawa and Basham (1965) and Utsu (1967), studied spectral amplitudes at 0.5-3.0 Hz frequencies and concluded that P-wave absorption beneath a seismic station at Resolute,

Canada was greater than that beneath other stations in northern Canada.

Tryggvason (1965) devised a least-squares method for simultaneously obtaining Rayleigh- wave attenuation coefficients and source amplitudes using several stations located at varying distances from an explosive source. Since he assumed the source radiation pattern in this method to be circular he had no need to determine that pattern or know the crustal velocity structure. In the same year Anderson et al. (1965) developed equations that allowed measured surface-wave attenuation to be inverted for models of shear-wave Q (Q_μ) variation with depth and applied it to long-period surface waves that were sensitive to anelasticity at upper mantle depths.

Sutton et al. (1967), studied radiation patterns for Pg and Lg phases recorded at several stations in the United States and found that focusing and regional attenuation differences affected both waves. They concluded that the nature of the tectonic provinces traversed by the waves was more important than initial conditions at the source in determining the observed radiation patterns.

3 REGIONAL Q VARIATIONS IN THE CRUST AND UPPER MANTLE

3.1 Introduction

One of the most interesting aspects of Q in the crystalline crust and upper mantle of the Earth is the large magnitude of its variation from region to region. Whereas broad-scale seismic velocities vary laterally at those depths by at most 10–15%, Q can vary by an order of magnitude or more. Figure 2 illustrates the large effect that regional Q variations can have on phases that travel through both the upper mantle (P and S waves) and the crust (Lg) by comparing records for paths across the eastern and western United States. Since variations in Q can be so large, seismic wave attenuation is often able to relate Q variations to variations in geological and geophysical properties that are not easily detected by measurements of seismic velocities. Factors known to contribute to Q variations in the crust and upper mantle include temperature and interstitial fluids.

In this section we will emphasize studies of Q variation conducted over regions sufficiently broad to contribute to our knowledge of crust/upper mantle structure and evolution. In so doing we neglect many studies that have provided useful information on crustal Q over small regions. We will first address the topic of Q and its regional variation in the crust. That section will include a summary of methods for determining various types of crustal Q and describe some results using those methods. The following subsection will discuss methods and results using seismic tomography to map regional variations of crustal Q.

3.2 Q or Attenuation Determinations for Seismic Waves in the Crust

Investigators have employed different methods, phases and frequency ranges to study the anelastic properties of the crust and upper mantle. At the higher frequencies and shorter distances often employed for crustal studies some researchers have emphasized determinations of intrinsic Q (Q_i), some have emphasized the scattering contribution (Q_s) and some have sought to determine the relative contributions of Q_i and Q_s. The importance of scattering became apparent from the groundbreaking of K. Aki (Aki, 1969) who first showed that the codae of various regional phases are composed of scattered waves. His work spawned a large literature on both theoretical and observational aspects of scattering that is discussed (Shearer, 2006) elsewhere in this volume.

The contributions of the intrinsic and scattering components to total attenuation, $1/Q_t$ can be described by

$$\frac{1}{Q_t} = \frac{1}{Q_i} + \frac{1}{Q_s} \tag{2}$$

where Q_i and Q_s refer respectively to intrinsic and scattering Q (Dainty, 1981). Richards and Menke (1983) verified that the contributions of intrinsic and scattering attenuation are approximately additive as described by equation (1). Seismologists often wish

to focus on Earth's intrinsic anelastic structure. To do so they must select a phase or work in a frequency range such that the effect of scattering can either be determined or is small relative to the effect of intrinsic Q.

This review deals almost entirely with intrinsic Q, but we will discuss one type of scattered wave (Lg coda) quite extensively. Although Lg coda is considered to consist predominently of scattered energy, theoretical and computational studies (discussed later) of scattered S-wave energy indicate that measured Q values for that wave largely reflect intrinsic properties of the crust.

All of the measurements that we discuss in this section can be placed in one of two major categories: (1) those in which seismic source effects cancel and (2) those in which assumptions are made about the seismic source spectrum. For category (1) the cancellation is most often achieved by using ratios of amplitudes recorded by two of more instruments. But it has also been achieved using ratios of amplitudes from different portions of a single time series. The primary application of the latter type of cancellation has been for the determination of Lg coda Q (Q_{Lg}^{C}). We divide this category into three parts that address regional phases, fundamental-mode surface waves and Lg coda. Category (2) permits studies of Q using a single station, but requires knowledge of the source depth, source mechanism and velocity model for the source region. We divide this category into two parts, one addressing regional phases and the other fundamental-mode surface waves.

Seismologists have measured the dispersion of body waves due to anelasticity and have successfully used that dispersion to infer values for body-wave Q. We will not cover that topic because it has been the subject of relatively few studies and has been applied mainly to small regions.

The following subsections discuss methodology and present some representative results using the cited methods as applied to the crust. Because the number of studies for continents is overwhelmingly greater than for oceans, most of discussion will pertain to continental regions. A few studies will, however, be described for oceanic regions.

3.2.1 Spectral decay methods in which source effects cancel – Regional phases

Regional phases include those P, S and Lg phases recorded at distances less than about 1000 km. The early portion of this sub-section mostly covers Q determinations for P and S phases but in cases where researchers measured Q_{Lg} as well as Q_P and Q_S all results will be presented. The latter part of this subsection will, however, be devoted exclusively to Lg since that phase has been widely used in recent years to study variations of Q over broad regions.

Several methods in which the source cancels utilize stations that lie on a common great-circle path with the seismic source but other methods are able to dispense with the need for great-circle path propagation. All studies, however, need to first remove the effect of wave-front spreading before measuring amplitude changes due to attenuation. In this subsection we will restrict our discussion to studies at frequencies that pertain totally or predominantly to the crust with occasional reference to the upper mantle for studies that include results for both the crust and upper mantle.

Regional and near-distance studies of P- and S-wave attenuation (or their respective quality factors Q_P and Q_S) often cancel the source by utilizing several stations at varying distances. Nuttli (1978), for example, measured body-wave attenuation for 10-Hz P and Lg waves in the New Madrid region of the central United States. He found that P waves at that frequency fall off as the inverse 1.4 power of epicentral distance and that the apparent Q for Lg is 1500, a value thought at that time to be identical with that for 1-Hz Lg. Nuttli (1980) studied wave propagation in Iran and found that the coefficients of attenuation for 1-Hz Pg, Sn and Lg waves in Iran were, on average, 0.0045 km^{-1}, a value similar to that found for California and much higher than that observed in eastern North America. 3-s Lg waves in Iran exhibited values of about 0.003 km^{-1}.

Thouvenot (1983) utilized explosion data recorded by a linear array in the French Massif Central and found that body-wave Q varied with frequency. At 20 Hz they found Q to increase approximately linearly with depth, from 40 to 600 between the surface and

a depth of 7 km.

In another approach, Carpenter and Sanford (1985) utilized microearthquakes in the magnitude range -0.9 - 0.3 recorded by a small instrument array in New Mexico to determine Q_P and Q_S at high frequencies (3 - 30 Hz). By measuring the slope of amplitude determinations with distance, they found that Q increases with epicental distance and can be modeled by a low-Q zone ($Q < 50$) of varying thickness overlying a high-Q half-space with an average Q_S of 535. They found that Q_P/Q_S ranged between 0.34 and 1.39.

More recently, amplitude measurements in which both the source and sensor reside in boreholes beneath any sediments or weathered layers have provided much-improved estimates of Q_P and Q_S. Abercrombie (1997) used borehole recordings to determine spectral ratios of direct P to S waves and found that they are well modeled with a frequency-independent Q_P distribution in the borehole increasing from 26 to 133 at depths between the upper 300 m and 1.5 to 3 km. Q_S increased from 15 to 47 in the same depth range. Abercrombie (2000), in another borehole study near the San Andreas Fault, found that attenuation on the northeastern side of the fault is about twice that on the southwestern side.

Lg is very useful for Q studies both because it travels predominantly in the crustal waveguide, providing Q information for a known depth interval, and is a large and easily recognizable phase. Even relatively small earthquakes can generate useable records; thus data, in many regions is plentiful. *Lg* can be represented by a superposition of many higher-mode surface waves or by a composite of rays multiply reflected in the crust. It is usually assumed that Q_{Lg} follows a power-law frequency dependence, $Q{=}Q_o f^{\eta}$, where Q_o is the value of Q_{Lg} at a reference frequency and η is the frequency dependence parameter at that frequency.

Lg travels through continental crust at velocities between about 3.2 and 3.6 km/s and is usually followed by a coda of variable duration. That coda is discussed in sub-section 4.2.3. Since the *Lg* wave consists of many higher modes studies often assume that, even though the radiation patterns for individual modes differ from one another, the totality of modes combine to form a source radiation pattern that is approximately circular. If that assumption is correct the source and stations need not necessarily line up along the same great-circle path to estimate Q.

Early determinations of Q_{Lg}, after correcting for wave-front spreading, compared observed attenuation with distance with theoretically predicted attenuation for the *Lg* phase and chose the theoretical curve (predicted by selected values of Q_o and η) which agreed best with observations. One such study (Nuttli, 1973) estimated the attenuation coefficent of 1-Hz *Lg* to be about 0.07 deg^{-1} and of 3-12 s waves to be about 0.10 deg^{-1} in the central United States. In other studies Street (1976) found that 1-Hz *Lg* in the northeastern United States attenuated at a slightly greater rate than in the central United States and Bollinger (1979) found that, in the eastern United States, the same phase attenuated at a rate similar to that found by Nuttli in the central United States.

Hasegawa (1985) studied the attenuation of 0.6- 20 Hz *Lg* energy in the Canadian Shield and found that Q for 1-Hz *Lg* could be described by $Q = 900f^{0.2}$ for a portion of the Canadian Shield. Campillo et al. (1985) studied 0.5-10 Hz data in France and found that Q variation with frequency could be described by $Q = 290\ f^{0.52}$. They attributed the low Q value either to sediments or to scattering in the lower crust. Chavez and Priestley (1986) studied *Lg* using events recorded by four stations in the Great Basin. They found that for explosions recorded by a linear array that $Q = 206\ f^{0.68}$ for $0.3 < f < 10.0$ Hz and for earthquakes recorded by four stations $Q{=}214 \pm 15f^{0.54\pm0.09}$ for $0.3 < f < 5.0$ Hz.

Chun et al. (1987) developed a two-station two-event method for determining Q_{Lg}. It yields values for interstation Q that are not adversely affected by site responses at the two stations and provides a value for the ratio of the responses. This is achieved by recording amplitudes of two waves that traverse the station pair in opposite directions. They applied the method to 0.6-10 Hz *Lg* waves in eastern Canada and found their attenuation coefficient (γ) to be described by the relation $\gamma(f) = 0.0008f^{0.81}\ km^{-1}$. They concluded that γ appears to be independent of frequency and contaminated by high-frequency coda energy of

S_n waves

Benz et al. (1997) studied four regions (southern California, the Basin and Range province, the central United States, and the northeastern United States and southeastern Canada) of North America in the frequency range 0.5-14.0 Hz. They found that Q_{Lg} at 1 Hz varies from about 187 in southern California to 1052 in the northeastern United States and southeastern Canada and about 1291 in the central United States. They also found that the frequency dependence of Q also varies regionally, being relatively high (0.55-0.56) in southern California and the Basin and Range and smaller (0-0.22) in the other three regions.

Xie and Mitchell (1990a) applied a stacking method to many two-station measurements of Q_{Lg} at 1 Hz frequency in the Basin and Range province. This method, first developed for single-station determinations of Lg coda Q (Q_{Lg}^C), will be discussed in the subsection on Lg coda. They found that Q_{Lg} $=(275 \pm 50) f^{(0.5 \pm 0.2)}$ and $Q_{Lg}^C = (268 \pm 50) f^{(0.5 \pm 0.2)}$.

Xie et al. (2004) extended the method to multiple pairs of stations in instrument arrays across the Tibetan Plateau. For an array in central Tibet (INDEPTH III) they found very low values for Q_o (~90) that they attributed to very high temperatures and partial melt the crust. An array in southern Tibet yielded even lower values, ~60, for Q_o in the northern portion of the array but higher values (~100) in a central portion and much higher values (>300) in the southernmost portion. Xie et al. (2006) used a two-station method to obtain more than 5000 spectral ratios for 594 interstation paths and obtained Q_o and η for those paths. They obtained tomographic maps of those values that are described in the subsection on tomographic mapping.

3.2.2 Spectral decay methods in which source effects cancel – Fundamental-mode Surface waves

When using fundamental-mode surface waves to study lateral variations of crustal Q_μ we need to measure the attenuation of relatively short-period (5-100s) amplitudes. In continents it has long been known that those waves may be biased by systematic errors associated with laterally varying elastic properties along the path of travel. These might be caused by lateral refraction over non-great-circle paths, focusing/defocusing and multipathing, effects that can lead to large systematic errors in measurements of surface-wave attenuation values. Two-station studies of fundamental-mode surface waves are especially susceptible to these types of error because researchers might incorrectly assume great-circle propagation along a path through the source and the two stations. Non-great-circle propagation would mean that surface-wave energy arriving at two stations along different great-circle paths could originate at different portions of the source radiation pattern. If that pattern is not circular the two-station method can produce attenuation coefficient values that are either too high or too low, depending on the points of the radiation pattern from which the waves originate.

Measurements for the situation in which a source and two stations lie approximately on the same great circle path have often been used to determine surface-wave attenuation. The method was described by Tsai and Aki (1969) and determines the average surface-wave Q between the two stations after correcting for the different wave front spreading factors at the two stations. They applied the method to many two-station paths from the Parkfield, California earthquake of June 28, 1966 and, using the formulation of Anderson et al. (1965), obtained a frequency-independent model of intrinsic shear-wave Q (Q_μ) with a low-Q zone that coincided with the Gutenberg low-velocity zone in the upper mantle. Love-wave Q was greater than 800 and Rayleigh-wave Q was greater than 1000 in the period range 20-25s.

Other studies using the method to obtain Q_μ models at crustal and uppermost mantle depths include those of Hwang and Mitchell (1987) for several stable and tectonically active regions of the world, Al-Khatib and Mitchell (1991) for the western United States and Cong and Mitchell (1998) for the Middle East.

Models have also been obtained in which Q_μ varies with frequency. That frequency dependence is described by the relation $Q_\mu = Q_o f^\zeta$ where ζ may vary with frequency (Mitchell, 1975) or with depth

(Mitchell and Xie, 1994). The inversion process for Q_μ in those cases requires appropriate extensions of the Anderson et al. (1965) equations. The process requires both fundamental-mode surface-wave attenuation data and Q or attenuation information for either an individual higher mode or the combination of higher modes that form the Lg phase. The process proceeds by assuming a simple one- or two- layer distribution of ζ and inverting the fundamental-mode data for a Q_μ model. ζ is adjusted until a Q_μ model is obtained that explains both the fundamental-mode and higher-mode attenuation data. Mitchell and Xie (1994) applied the method to the Basin and Range province of the western United States. Example Q_μ models for which ζ varies with depth (Mitchell and Xie, 1994) appear in Figure 3.

Other surface-wave studies for which the source is cancelled are those that use many stations at various distances and azimuths and simultaneously solve for surface-wave attenuation coefficient values and seismic moments for particular periods by linear least-squares. Tryggvason (1965) first did this, as described in our section on early studies, using explosions and assuming circular radiation patterns. Tsai and Aki (1969) extended this method to use earthquake sources. They had to know the earthquake's depth and focal mechanism in order to correct for the effect of azimuthally-varying source radiation patterns. They applied it to surface waves generated by the June 28, 1966 Parkfield, California earthquake. This process was later applied to the central United States (Mitchell, 1973; Herrmann and Mitchell, 1975), and the Basin and Range province of the western United States (Patton and Taylor, 1989).

A non-linear variation of the Tsai and Aki method (Mitchell, 1975), represents a nuclear explosion with strain release by a superposition of an explosion (with a circular radiation pattern) and a vertical strike-slip fault (represented by a horizntal douple-couple). Variations of the orientation of the double couple and its strength relative to the explosion produce patterns that approximate a wide variety of radiation patterns. The inversion solves for the moment of the explosion, the orientation of the double-couple, the strength of the double-couple relative to the explosion and an average attenuation coefficient value for each period of interest. Mitchell applied the method to two nuclear events in Colorado as recorded by stations throughout the United States and found that Q_μ in the upper crust of the eastern United States is about twice as high as it is in the western United States at surface-wave frequencies.

The first attempts at mapping regional variations of attenuation or Q utilized crude regionalizations (two or three regions) based upon broad-scale geological or geophysical information. Yacoub and Mitchell (1977), applied the method of Mitchell (1975) to earthquakes and obtained regionalized surface-wave attenuation values over much of Eurasia. They divided Eurasia into two broad regions, one stable and one tectonically active, based upon geological information, and used the equation

$$A_o(\omega) = A_t(\omega) \exp\left[-\sum_1^N \gamma_i(\omega) X_i\right] \qquad (3)$$

where $A_o(\omega)$ represents observed spectral amplitudes corrected for geometrical spreading, $A_t(\omega)$ indicates theoretical amplitudes when attenuation is absent, N is the number of regions traversed by the great circle path between the source and receiver, $\gamma_i(\omega)$ is the attenuation coefficient value for the i^{th} region and X_i is the distance, in km, traversed in the i^{th} region. They found that Rayleigh-wave attenuation coefficients in the tectonically active portion of Eurasia at periods smaller than 20 s were higher than those for the stable portion and that the regionalization considerably reduced the standard errors of the attenuation coefficient values for both regions.

Canas and Mitchell (1978) measured Rayleigh-wave attenuation coefficients in the Pacific with a two-station method using various pairs of island stations. They then divided the Pacific into three regions based upon reported ages of the sea floor and, by a least-squares inversion of equation 2, obtained regionalized attenuation coefficients for much of the Pacific basin. The coefficients obtained for the three regions (0-50 My, 50-100 My and >100 My in age) showed decreasing Rayleigh-wave attenuation values with increasing age of the sea floor. Inversions of the attenuation coefficients for the three regions produced Q_μ^{-1} models with relatively high standard er-

rors for the three regions, but showed that average Q_μ^{-1} for the crust decreases from about 8.0 x 10^{-3} to 6.0 x 10^{-3} (or Q_μ increases from about 125 to about 167). Q_μ for the upper mantle also increased with age throughout both the lithosphere and asthenosphere.

A second oceanic study (Canas and Mitchell, 1981), using the same two-station methodology and a smaller data set, found that Rayleigh-wave attenuation beneath the Atlantic, like that beneath the Pacific, decreases with increasing age of the sea floor, and that Q_μ values at the same depths were higher beneath the Atlantic than beneath the Pacific. They concluded that, since plate spreading rates were lower beneath the Atlantic, that internal friction, Q_μ^{-1}, is related to long-term creep in the upper mantle.

3.2.3 Spectral decay methods in which source effects cancel – *Lg* coda

Lg coda, like direct *Lg*, is sensitive to properties through a known depth range (the crust) in which it travels and is a large phase for which data are plentiful. In addition, since the coda of *Lg* is comprised of scattered energy, it can continue to oscillate for several hundred seconds following the onset of the direct *Lg* phase, thus making it possible to stack spectral amplitudes for many pairs of time windows to make a Q estimate. Other positive aspects of using *Lg* coda for Q studies are that the averaging effect of scattering stabilizes Q_{Lg}^C determinations and, if stacking methods are utilized to determine Q for *Lg* coda, site effects cancel (Xie and Mitchell, 1990a).

Two methods have been applied to *Lg* coda to make Q determinations. The first of these was developed by Herrmann (1980) and applied by Singh and Herrmann (1983) to data in the United States. The method extended the coda theory of Aki (1969) utilizing the idea that coda dispersion is due to the combined effects of the instrument response and the Q filter of the Earth. The two studies provide new information on the variation of of Q across the United States. Herrmann later realized, however, that his method did not take into consideration the broadband nature of the recorded signal and overestimates Q by about 30% (R.B. Herrmann, personal communication).

Xie and Nuttli (1988) introduced a method, termed the Stacked Spectral Ratio (SSR) method which stacks spectra from several pairs of windows along the coda of *Lg*. That process leads to

$$R_k = f^{1-\eta}/Q_o, \tag{4}$$

as the expression for the SSR, or in logarithmic form

$$\log R_k = (1-\eta)\log f_k - \log Q_o + e, \tag{5}$$

from which Q_o and η can be obtained by linear regression. f_k, Q_o, η and e in these equations are, respectively, a discrete frequency, the value of Q at 1 Hz, the frequency dependence of Q at frequencies near 1 Hz, and an estimate for random error. This stacking process provides stable estimates of Q_o and η with standard errors sufficiently low to allow tomographic mapping of those quantities. A detailed description of the SSR method appears in Xie and Nuttli (1988) and more briefly in Mitchell et al. (1997).

Three examples of seismograms that include *Lg* and its coda for Eurasian paths appear in Figure 4. Measured values of Q_o decrease from top to bottom in the figure. Note that the SSR plot can be fit over a broad frequency range with a straight line on a log-log plot. The value at 1 Hz provides an estimate of $1/Q$ at that frequency and the slope of the line gives an estimate for η. The top trace is for a relatively high-Q_o (701) path to station HYB in India, the bottom trace is for a low-Q_o (208) path to station LSA in Tibet and the middle trace is from a path to station BJT in northern China where Q_o (359) is intermediate between the other two. The traces show a progression of decreasing predominant coda frequencies and amplitudes with decreasing Q value.

SSR plots appear to the right of each trace. Portions of all three traces form an approximate straight line on a log-log plot that can be fit by least squares. The value and slope of the best- fitting line at 1 Hz yields, respectively, values for Q_o and η. Inversions of sets of those values over a broad region yield tomographic maps of those quantities.

Past studies have shown that several factors may contribute to reductions in Q_o; these include thick accumulations of young sediments (Mitchell and

Hwang, 1987) and the presence of a velocity gradient rather than a sharp interface at the crust/mantle boundary (Bowman and Kennett, 1991; Mitchell et al., 1998). In addition, decreasing depth of the Moho in the direction of Lg travel or undulations of the Moho surface can be expected to decrease measured Q_{Lg} or Q_{Lg}^{C} whereas increasing depth would produce larger values. These factors may cause determinations of correlation coefficients between Q_{Lg} or Q_{Lg}^{C} and various crustal or mantle properties to be relatively low whenever they are determined (e.g., Zhang and Lay, 1994; Artiemeva et al., 2004).

3.2.4 Spectral decay methods for which assumptions are made about the source spectrum – Regional phases

Hough et al. (1988) studied S waves traveling over relatively short distances near Anza, California and defined the instrument-corrected acceleration spectrum at a station located a distance r from the source as

$$A(r, f) = A_o e^{-\pi t^*}, \tag{6}$$

where t^* is defined as

$$t^* = \int_{path} \frac{dr}{QV}, \tag{7}$$

for which Q is the quality factor for the phase of interest, V is the wave velocity and the integral is taken along the ray path. For crustal studies it is common to assume that Q is constant along the path, in which case

$$t^* = \frac{t}{Q}, \tag{8}$$

where t is the travel time.

Hough et al. (1988) defined A_o as

$$A_o = (2\pi f)^2 S(f) G(r, f), \tag{9}$$

where $S(f)$ is the source displacement spectrum and $G(r, f)$ is the geometrical spreading factor which, if we assume frequency independent propagation in a homogeneous medium, is $1/r$ for body waves. At higher frequencies these methods assume a spectral fall-off rate (such as ω^{-2} or ω^{-3}) and attribute additional fall-off to attenuation. Since a large body of data supports the ω^{-2}, or Brune, model (Brune, 1970) that is the one most commonly used. Taking the natural logarithm of equation (6) leaves

$$\ln A(f) = \ln A_0 - \pi f t^*. \tag{10}$$

For the frequency-independent case this equation defines a straight line with an intercept of $ln\ A_o$ and a slope of $-\pi t/Q_o$.

Anderson and Hough (1984) hypothesized that, to first-order, the shape of the acceleration spectrum at high frequencies can be described by

$$\alpha(f) = A_o e^{-\pi \kappa f} f > f_E \tag{11}$$

where f_E is the frequency above which the spectral shape is indistinguishable from spectral decay and A_o depends on source properties and epicentral distance. They found that κ increased slowly with distance, an observation consistent with a Q model of the crust that increases with depth in its shallow layers and that it was systematically smaller on rock sites than at alluvial sites. Hough et al. (1988) studied κ as a function of hypocentral distance, as well as site and source characteristics and found that $\kappa(0)$ differed for sites at Anza and the Imperial Valley in California but that $d\kappa/dr$ was similar for the two regions. Their interpretation was that $\kappa(0)$ was a component of attenuation that reflects Q_i in the shallow portion of the crust while $d\kappa/dr$ was due to regional structure at great depth.

Hasegawa (1974) used this method to estimate a frequency-independent Q for strong motion S waves in the Canadian Shield and found that Q increased with distance. He attributed that result to increasing shear-wave Q with depth in the crust. Using the same assumptions Modiano and Hatzfeld (1982) found that measured shear-wave Q in the Pyrenees increased with source depth and that S-wave Q was higher than P-wave Q by a factor of 1.6. Al-Shukri et al. (1988) utilized the same method in the New Madrid zone of the central United States and found that Q is lower for paths predominantly within the region of earthquake activity than for paths outside it.

Shi et al. (1996) studied Q_{Lg} variation for five tectonically different regions of the northeastern United

States. They used eight pairs of co-located earthquakes to determine accurate source spectrum corner frequencies by applying an empirical Green's function method to Pg and Lg or Sg phases. Based upon the corner frequencies, Sg or Lg displacement spectra were used to obtain values of Q and η values for 87 event-station paths at frequencies between 1 and 30 Hz. 1-Hz Q_o values for the five regions vary between 561 and 905 while η varies between 0.40 and 0.47. Table 1 shows Q_o and η values for the five regions and compares them with 1-Hz values from a tomographic study (See the section on tomographic mapping) of Q_{Lg}^C for that region obtained by Baqer and Mitchell (1998).

3.2.5 Spectral decay methods for which assumptons are made about the source spectrum – Fundamental-mode Surface waves

A multi-mode spectral method has yielded simple crustal models (two or three layers) of shear wave Q (Q_μ) in a few regions. The method assumes a flat source spectrum and tries to match theoretical amplitude spectra to two sets of observed spectral amplitude data, one corresponding to the fundamental mode and the other to the superposition of higher modes that forms the longer-period (3-10 s) component of the Lg phase. The higher modes travel faster than all but the longest-period fundamental-mode energy observed on records for relately small events that are used with this method.

The first study using that method (Cheng and Mitchell, 1981) compared upper crustal Q_μ for three regions of North America and found values of 275 for the eastern United States, 160 for the Colorado Plateau, and 85 for the Basin and Range province. Kijko and Mitchell (1983) applied the method to the Barents Shelf, a region of relatively high-Q crystalline crust overlain by low-Q sediments. They found the method to be sensitive to Q_μ in the sediments and upper crust but insensitive to Q_μ in the lower crust and to P-wave Q at all depths. Cong and Mitchell (1998) obtained models in which Q_μ is very low at all depths beneath the Iran/Turkish Plateaus and somewhat higher, but still much lower than expected beneath the Arabian Peninsula. Models they obtained using the multi-mode method, agree well with those they obtained using the two-station method.

Jemberie and Mitchell (2004) applied the method to China and peripheral regions and obtained three-layer crustal models with low Q_μ and wide variation across China and values that decrease with depth beneath regions such as southeastern China and increase with depth beneath other regions such as the eastern Tibetan Plateau. The following section on Tomographic Mapping of Crustal Q presents Q_μ maps obtained in that study.

3.3 Tomographic Mapping of Crustal Q

Seismologists are currently attempting to map variations of Q and its frequency variation in the Earth in as much detail as possible. For continents researchers have obtained tomographic maps for several broad regions using Lg coda, the direct Lg phase and surface waves. Studies of smaller regions, such as volcanoes and geothermal areas, have utilized P and S waves (e.g., Hough et al., 1999). In this review, we will restrict our discussion to the more broad-scale studies.

An earlier section described three early regionalized studies of surface-wave in the late 1970s and early 1980s, one for continental paths and two for oceanic paths in which the Eurasian continent, the Pacific Ocean and Atlantic Ocean were coarsely divided into two or three regions. Since then tomographic mapping using Lg coda has made possible a much finer regionalization of crustal Q in continents. This section will discuss tomography results for continents and for one oceanic region using either direct Lg, fundamental-mode surface waves, P and S waves.

We emphasize Lg coda since tomographic maps of Q_{Lg}^C, all obtained for the same frequency, and using the same methodology, are available for all continents but Antartica. This commonality in phase, frequency and method allows us to compare Q from continent to continent and also to other geophysical and geological properties. These comparisons have contributed to our understanding of the mechanisms for seismic-wave attenuation.

Earlier sections have indicated that Lg coda has several properties that make it useful for tomographic studies. First, it is usually a large phase making it easily available for study in most regions of the world. Second, it is a scattered wave and the averaging effect of that scattering makes Lg coda relatively insensitive to focusing. Third, the stacked spectral ratio (SSR) method used to determine Q_o and η tends to cancel site effects. Fourth, although it is a scattered wave, measurements of Q for seismic coda have been shown theoretically and computationally to yield measures of intrinsic Q. That allows researchers to interpret Q variation in terms of Earth structure and evolution.

As indicated earlier, Lg coda Q (Q_{Lg}^C) is typically assumed to follow a power-law frequency dependence, $Q_{Lg}^C = Q_o f^\eta$, where Q_o is the Q value at 1 Hz and η is the frequency dependence of Q near 1 Hz. Tomographic maps of the 1-Hz values of Q_{Lg}^C (Q_o and η) with nearly continent-wide coverage are now available for Eurasia (Mitchell et al., 1997, 2006), Africa (Xie and Mitchell, 1990b), South America (DeSouza and Mitchell, 1998) and Australia (Mitchell et al., 1998). In North American broad-scale determinations of Q_{Lg}^C are currently restricted to the United States (Baqer and Mitchell, 1998). Tomographic studies have also been completed for more restricted regions using the direct Lg phase in Eurasia, North America, and South America. and high-resolution tomographic maps of Q for P and S waves are available for southern California. For oceanic regions tomographic mapping of Q variations, to our knowledge, is currently available only for P-waves in one broad portion of the East Pacific rise (Wilcock et al., 1995).

Sarker and Abers (1998) showed that, for comparative studies, it is important that researchers use the same phase and methodology in comparative Q studies. The Lg coda Q maps presented here adhere to that principle; thus the continental-scale maps of Q_o and η for Lg coda at 1 Hz that are available can be considered to provide the closest thing to global Q coverage at crustal depth that currently exists. The maps also present the possibility for comparisons of Q_o variation patterns with variations of seismic velocity, temperature, plate subduction, seismicity, the surface velocity field and tectonics when that information is available.

A discussion of the inversion method for mapping Q_o and η appears, in detail, in Xie and Mitchell (1990b), and more briefly, in Mitchell et al. (1997). The method assumes that the area occupied by the scattered energy of recorded Lg coda can be approximated by an ellipse with the source at one focus and the recording station at the other, as was shown theoretically by Malin (1978) to be the case for single scattering.

Xie and Mitchell (1990b) utilized a back-projection algorithm (Humphreys and Clayton, 1988) to develop a methodology for deriving tomographic images of Q_o and η over broad regions using a number, N_d, of Q_o or η values determined from observed ground motion. Figures 5a, 8a, 9a, 10a, and 11a show the ellipses that approximate data coverage for the event-station pairs used in Q_{Lg}^C studies of Eurasia, Africa, South America, Australia and the United States. The inversion process assumes that each ellipse approximates the spatial coverage of scattered energy comprising late Lg coda. The areas of the ellipses grow larger with increasing lag time of the Lg coda components. The ellipses in the figure are plotted for maximum lag times used in the determination of Q_o and η. Ideally, each inversion should utilize many ellipses that are oriented in various directions and exhibit considerable overlap in order to obtain the redundancy needed to obtain the best possible resolution for features of interest.

The continents are divided into N_c cells with dimensions ranging from 1.5^o by 1.5^o to 3^o by 3^o, based upon theoretical resolution over which Q_o will have constant value. The Q_n value for each trace corresponds to the areal average of the cells covered by its associated ellipse. If the area over which the ellipse for the n^{th} trace overlaps the m^{th} cell is S_{mn} then

$$\frac{1}{Q_n} = \frac{1}{S_n} \sum_{m=1}^{N_c} \frac{S_{mn}}{Q_m} + \epsilon_n n = 1, 2, \cdots, N_d \qquad (12)$$

where

$$S_n = \sum_{j=1}^{N_c} S_{jn}, \qquad (13)$$

and e is the residual due to the errors in the measurement and modeling of Lg coda.

A map of the frequency dependence of Q_{Lg}^C at 1 Hz is obtained using the N_d values for Q_o and η obtained at that frequency to estimate Q_{Lg}^C at another frequency which we take to be 3 Hz. The 3-Hz values become Q_n in equation 12 and an inversion yields a map of Q_{Lg}^C at that frequency. We then utilize he equation

$$\eta = \frac{1}{\ln 3} \ln \frac{Q(f)_{3Hz}}{Q_o}, \tag{14}$$

to obtain a map of the frequency dependence of Q_{Lg}^C at 1 Hz.

The point spreading function (psf) suggested by Humphreys and Clayton (1988) provides an excellent measure of resolution when applying the back-projection method. It is obtained by constructing a model in which Q^{-1} is unity in a cell of interest and zero in all other cells. Determination of average Q_o values for all elliptical areas for the various models then yield synthetic data sets that can be inverted to see how Q^{-1} varies around each selected cell. This inversion yields the psf pertaining to the region of the selected and surrounding cells. The area and falloff with distance from the central cell provides an estimate of resolution.

Random noise in the coda of Lg will, of course, affect images obtained for Q_o and η. That effect can be tested empirically using the sample standard error in Q_n caused by randomness of the $SSRs$ (Xie and Mitchell, 1990b). If the standard error of Q_n is denoted by Q_n, $n = 1, 2, \ N_d$, and if we assume that Q_n gives a good measure of the absolute value of real error preserved in the Q_n measurements, we can construct several noise series for which the m^{th} member has an absolute value equal to Q_n and a sign that is chosen randomly. The n^{th} term of the noise series is added to Q_n and the sums of the two series are then inverted to obtain a new Q_m image from which the original one is subtracted to yield an error estimate of the Q_n values. Since the sign of $Q_n$was determined using a random binary generator, the process should be repeated several times to obtain an average error estimate.

It is important to emphasize that, because Lg coda consists of scattered energy, it must be distributed, for each event-station pair, over an area surrounding the great-circle path between the source and receiver. Because of this areal coverage, our maps may not include effects of Lg blockage in regions where such blockage has been reported. We may have no data from blocked paths, but are likely to have other paths, such as those sub-parallel to the blocking feature or for which the source or recording station, represented by one focus of the scattering ellipse, lies near the blocking feature. In both cases portions of the scattering ellipses may overlap the blocking feature, but that feature will not substantially contribute to the values we obtain for Q_o and η.

A comparison of mapped Q_o for all continents (Figures 5b, 8b, 9b, 10b and 11b) shows that it is typically highest in the stable portions of continents and lowest in regions that are, or recently have been, tectonically active. Exceptions occur, however, especially for stable regions. For instance, the Arabian Peninsula, although being a stable platform shows Q_o variations between 300 and 450, values that are one-half or less of maximum values in other Eurasian platforms. Other regions showing lower than expected Q_o include the Siberian trap region of northern Siberia and the cratonic regions of Australia.

The frequency dependence values of Q_{Lg}^C (η) in Figures 5c, 8c, 9c, 10c and 11c appear to show consistent relationships to Q_o in some individual continents. For instance, in both Africa and South America high-Q regions are typically regions of low η. That same relationship, however, does not occur consistently in Eurasia, Australia or the United States. η is high, for instance, throughout much of the northern portions of Eurasia where Q_o is mostly high but is low in California, Kamchatka and a portion of southeast Asia where Q_o is very low.

3.3.1 Q_{Lg}^C, Q_{Lg} and Q_μ tomography in Eurasia

Figure 5 shows maps of data coverage, Q_o and η across virtually all of Eurasia (Mitchell et al., 2006). These maps represent a major increase in data coverage for northeastern Siberia, southeastern Asia, India and Spain, compared to those of an earlier study (Mitchell et al., 1997) and provide additional redundancy in regions where there was earlier coverage. As indicated by Figure 5a, the data coverage is excellent

for virtually all of Eurasia. The Q_o map contains several features that appear to correspond to features on the tectonic map of Figure 6. The single most prominent feature of the Q_o map is the broad band of low values in the Tethysides orogenic zone shown in Figure 5b. It extends across southern Eurasia from western Europe to the Pacific Ocean and its southern portions appear to be related to subduction processes occurring at the present time. While Q_o is generally high in the platforms of northern Eurasia and India (600-950), it is very low in the Kamchatka Peninsula and regions directly north of there. A conspicuous region of relatively low Q_o lies in central Siberia and corresponds, spatially to the Siberian Traps shown in Figure 6.

The four zones with lowest Q values lie in the Kamchatka Peninsula in northeastern Siberia, the southeastern portions of the Tibetan Plateau and Himalaya, the Hindu Kush (just north of India) and western Turkey. All of these regions are also very seismically active, a correspondence that suggests that low-Q regions are associated with regions of high crustal strain.

Other low-Q regions appear to be related to upper mantle processes. A comparison of Figure 5b with wave velocities at long periods (Ekström et al., 1997), that are not sensitive to crustal properties, shows a correspondence of low Q regions with regions of low upper mantle velocities. This is most apparent for the broad band of low Q values throughout southern Eurasia but also occurs in the Siberian trap region of Siberia. Both the low-Q and low-velocity regions largely coincide with high upper mantle temperatures (Artemieva and Mooney, 2001).

Patterns of η variation in Figure 5c, in contrast to those of Q_o variation, show no clear-cut relationship to tectonics. They similarly show no relation to patterns of Q_o variation. For instance, Kamchatka has low Q_o and low η while Spain has low Q_o and high η.

Seismologists have completed other tomographic studies for portions of Eurasia using Q_{Lg} and shear-wave Q (Q_μ). Xie et al. (2006) used a two-station version of the SSR method to determine more than 500 spectal ratios over 594 paths in eastern Eurasia. They were able to determine tomographic models for Q_o and η with resolution ranging between 4^o and 10^o in which Q_o varies between 100 and 900.

Using the single-station multi-mode method (Cheng and Mitchell, 1981), Jemberie and Mitchell (2004) obtained tomgraphic maps of shear-wave Q (Q_μ) for depth ranges of 0-10 km and 10-30 km (Figure 7). Although large standard errors accompany those determinations several features of their variation patterns, such as the low-Q regions in southern Tibet resemble the map of Q_o variations (Figure 5b). The maps of Figure 7 indicate that Q_μ varies between about 30 and 280 in the upper 10 km of the crust and between about 30 and 180 at 10-30 km depth. The maps indicate that Q_μ increases with depth in some regions, such as southern Tibet, and decreases in others, such as southeastern China.

3.3.2 Q_{Lg}^C and Q_{Lg} tomography in Africa

Xie and Mitchell (1990b), in the first tomographic study of Lg coda, determined Lg_o and η for continental Africa. Figure 8 shows maps of data coverage, Q_o and η for that entire continent (Xie and Mitchell, 1990b). Because of low seismicity rates in the western and northern parts of Africa, data coverage is only moderate to poor in those regions (Figure 8a).

The feature of the Q_o map of Africa (Figure 8b) that is most obviously related to tectonics is the low-Q region that broadly coincides with the East African rift system. The three high- Q regions correspond to Precambrian cratons: the West African Craton in the northwest, the East Sahara Craton in the northeast, and the Kalahari Craton in the south. The Congo Craton, situated just to the north of the Kalahari Craton does not show up as a region of high Q. This is probably due to the presence of a broad and deep basin of low-Q sedimentary rock, a factor shown likely to significantly reduce Q_o (Mitchell and Hwang, 1987).

Low Q_o values also occur in the Atlas Mountains (Cenozoic age) of northern Africa, the Cape Fold Belt (Permo-Triassic age) at the southern tip of Africa and the Cameroon Line (Miocene age) which is oriented in a NNE-SSW direction from the point where the western coast changes direction from east-west to north-south. All of those features are on the periph-

ery of the continent where there may be large uncertainty in the measured values of Q_o and η but there appears to be little question that, like Eurasia, the Q_o values increase with the length of time since the time of the most recent tectonic or orogenic episode.

The relation between Q_o and η is quite clear here. Low values of η (Figure 8c) occur where Q_o is high and higher values of η occur where Q_o is low. η, however, in the East African rift differs little from immediately surrounding regions.

3.3.3 Q_{Lg}^C and Q_{Lg} tomography in South America

Figure 9 shows data coverage, and values of Q_o and η obtained for South America DeSouza and Mitchell (1998). The data coverage (Figure 9a) is excellent throughout western South America where seismicity is high but poor in eastern regions, especially the most easterly regions, where there are few earthquakes. Figure 9b indicates that the low-Q (250-450) portion of South America is associated with the tectonically active western coastal regions. The lowest Q_o values occur along the coast between 15^o and 25^o S latitude where the level of intermediate-depth seismicity is highest in the continent. The slab in this region also dips steeply ($> 20^o$) and significant volcanism occurs (Chen et al., 2001). Davies (1999) had studied the role of hydraulic fractures and intermediate-depth earthquakes in generating subduction zone magmatism. He suggested that the level of intermediate-depth earthquakes was high because liberated fluids favored brittle fracture in response to stresses acting on the slab. Q levels may be low there because earthquake activity creates a degree of permeability that allows dehydrated fluids to be transported to the mantle wedge.

The relation between Q_o and η is virtually the same as that for Africa. Low values of η (Figure 9c) occur where Q_o is high and higher values of η occur where Q_o is low.

Ojeda and Ottemöller (2002), developed maps of Lg attenuation for most of Colombia at various frequencies in the 0.5-5.0 Hz range. Using 2928 ray paths, they were able to delineate regional variations of Q_{Lg} within that relatively small region. Their average Q_o value of 230 is significantly smaller than the values, between 300 and 400, found by DeSouza and Mitchell (1998) for Q_{Lg}^C in the same region. This difference may indicate that Q_{Lg} values in Columbia are due to contributions from both intrinsic absorption and scattering effects whereas Q_{Lg}^C is dominated by intrinsic absorption. This difference is consistent with several theoretical and numerical studies of S-wave attenuation (e.g. (Frankel and Wennerberg, 1987; Hoshiba, 1991; Zeng, 1991; Zeng et al., 1991)).

3.3.4 Q_{Lg}^C tomography in Australia

Figure 10 shows the data coverage and values of Q_o and η obtained for Australia (Mitchell et al., 1998). Data coverage (Figure 10a) there was the poorest of the five continents where Q_{Lg}^C was mapped over continent-scale dimensions. Q_o variation there is consistent, however, with the other studies and, for all but peripheral regions where systematic measurement errors can be high, it displays a clear relationship with past tectonic activity. Q_o in Australia (Figure 10b) is unusually low for a stable continental region. Highest values are in the range 550-600 in the southeastern corner of the continent (the Yilgarn Block) and along the southern coast (the Gawler Block). Values between 400 and 500 characterize much of the remaining cratonic crust. This compares with values of 800 and higher in most of the African and South American cratons. The youngest crust lies in eastern Australia where Q_o is between 350 and 400. An orogeny occurred there during the Devonian period and another occurred in the eastern portion of that region during the Permian period. Low Q_o values in the most westerly point of the continent and along the northern coast are probably due to very poor data coverage there (Figure 10a) and are probably meaningless.

Bowman and Kennett (1991) had earlier found low values for Q_{Lg} in north-central Australia and were able to explain them if the crust-mantle transition was a gradient rather than a sharp interface. They found that a velocity gradient with an approximate 25-km thick transition could explain their observations. Mitchell et al. (1998) found that they, with computations using one-dimensional models, could

explain reductions in Q_o up to about 20%, but not the 30% or greater reductions found in Australia. They suggested that the additional discrepancy might be explained if the crust-mantle transition varied in depth or thickness over broad region.

Low values of η are mostly associated with low values of Q_o and vice versa (Figure 10c). This is opposite to the relations between η and Q_o found in Africa and South America.

3.3.5 Q_{Lg}^C, Q_{Lg} and P/S tomography in North America

Figure 11 shows the data coverage, Q_o, and η values obtained for the United States (Baqer and Mitchell, 1998). Coverage (Figure 11a) is best in the western portions of the country, but is also reasonably good in the central and eastern portons. Figure 11b shows that Q_o is lowest (250-300) in California and the Basin and Range Province. That low-Q region forms the core of a broader region of low Q_o values that extends approximately to the western edge of the Rocky Mountains. Q_o in the Rocky Mountains and much of the Great Plains ranges between about 450 and 600. A high-Q (mostly 600-700) corridor extends from Missouri the north Atlantic states and New England. Q_o in New York and peripheral regions is somewhat higher (700-750).

The Q_{Lg}^C values of Baqer and Mitchell (1998) can be compared to those in studies of Q_{Lg} in two regions of the United States. One of these is the study of Shi et al. (1996) that was discussed earlier and for which values appear in Table 1. The values of Shi et al. are given numerically in one of their figures, whereas those of Baqer and Mitchell were estimated visually from the maximum and minimum values of Q_o (Figure 11b) in the region that corresponds to the region mapped by Shi et al. which lists that range of values. The agreement between the two sets of values is quite good. η in the map of Baqer and Mitchell (1998) is between 0.45 and 0.50 everywhere in Figure 11c. These values also correspond well to values in the map of Shi et al. The excellent agreement of Q_o and η between the mappings of Shi et al. and Baqer and Mitchell suggests that direct Lg is not losing significant energy by scattering and, consequently, energy loss by intrinsic absorption is the dominant factor in wave attenuation in the crust of the northeastern United States. The only correlation between Q_o and η in Figures 11b and 11c that can be made is for the westernmost part of the country where, like Australia, low η values appear to be associated with low values of Q_o.

Two research groups have studied the three-dimensional structure of P-wave and S-wave attenuation in southern California. Schlotterbeck and Abers (2001) fit theoretical spectra to observed spectra using the least-square minimization method of Hough et al. (1988), and determined t^* for P and S waves at frequencies between 0.5 and 25 Hz. Their inversions showed that P and S results were in substantial agreement, showed spatial variations, and correlated with regional tectonics. At upper crustal depths they found Q to be <500 in the Los Angeles Basin and Transverse Ranges and about 1000 in the Mojave Desert. At lower crustal depths they found Q_P to be about 700 and Q_S to be about 400 beneath the Salton Trough whereas the same properties were about 450 and 590 beneath the San Gabriel Mountains. They attributed the low Q beneath the Salton Trough to elevated temperature or partial melt resulting from active rifting and the low Q beneath the San Gabriel Mountains to elevated temperatures associated with active mountain building.

A second tomographic study of Q_{Lg} in the United States was conducted in the Basin and Range province (Al-Eqabi and Wysession, 2006) using a genetic algorithm technique. They found that Q_{Lg} increases (234-312) in a southwest-northeast direction across the Basin and Range in good agreement with the variation of Q_{Lg}^C reported by (Baqer and Mitchell, 1998).

The second study (Hauksson and Shearer, 2006) also determined t^* from $P-$ and $S-$wave spectra. They assumed that t^* consists of the sum of the whole-path attenuation and the local site effect at each recording station and utilize an expression of Eberhart-Phillips and Chadwick (2002) for the velocity spectrum. The inversion, in addition providing t^*, yields parameters defining the velocity amplitude spectra. They determined t^* for about 340,000 seismograms from more than 5000 events of t^* data

to obtain three-dimensional, frequency-independent crustal models for Q_P and Q_S in the crust and uppermost mantle in southern California. They found that both Q_P and Q_S generally increase with depth from values of 50 or less in surface sediments to 1000 and greater at mid-crustal depths. Their models reflect major tectonic structures to a much greater extent than they reflect the thermal structure of the crust.

As part of a broader study of Lg wave propagation in southern Mexico Ottemöller et al. (2002) used formal inversion methods to separately obtain tomographic maps of Q_{Lg} at three frequencies (0.5, 2.0 and 5.0 Hz) using 1^o by 1^o cells. Because of uneven path coverage in southern Mexico they applied regularization conditions to their inversion equations. They found lower than average Q_{Lg} in the Gulf of Mexico coastal plain and the area east of 94^oW. They found average Q_{Lg} values in the northern portion of the Pacific coastal region within their area of study and below average Q_{Lg} in the southern portion. An average Q_{Lg} for the region of study could described by the relation $Q_{Lg}(f) = 204f^{0.85}$.

3.3.6 Q_P variation near ocean ridges

Wilcock et al. (1995) developed a spectral technique by which they determined the attenuation of P waves in an active-source experiment centered at the East Pacific Rise at the latitude 9^o30'N. It is, to date, the only tomographic study of crustal Q variation in an oceanic region. They obtained over 3500 estimates of t^*, the path integral of the product of Q^{-1} and P-wave velocity where both quantities are variable along the path. Wilcock et al. display plots of both cross-axis as well as along-axis structure for upper crustal and lower crustal Q^{-1} structure. Within the ridge magma chamber Q reaches minimum values of 20-50 which extend to the base of the crust. Off the ridge axis they find that Q in the upper crust is 35-50 and at least 500-1000 at depths greater than 2-3 km. Figure 12 shows along-axis variations of upper crustal structure.

3.3.7 Variation of Crustal Q with time

Several investigators (e.g., Chouet, 1979; Jin and Aki, 1986) have reported temporal variations of Q over time scales of a few years. Although this observation has be reported several times, it continues to be controversial. Spatial patterns of Q variation and their apparent relation to time that has elapsed since the most recent episode of tectonic activity in any region, however, suggest that temporal variations of Q over very long periods of time can easily be detected. Mitchell and Cong (1998) found that variation for Q_{Lg}^C at 1 Hz extends between roughly 250, for regions that are currently tectonically active, and about 1000 for shields that have been devoid of tectonic activity for a billion years or more (Figure 13).

Mitchell et al. (1997) explained those observations as being due to variable volumes of fluids in faulted, fractured and permeable rock. Fluids enhance the rate of attenuation of seismic waves because the waves must expend energy to push those fluids through permeable rock as they propagate. Figure 13 points to an evolutionary process in which fluids are relatvely abundant in tectonically active regions due to generation by hydrothermal reactions at high temperatures. With time, fluids are gradually lost, either by migration to the Earth's surface or absorption due to retrograde metamorphism. This process causes low Q values early in the tectonic cycle and gradually increasing values at later times as the fluids dissipate.

References

Abercrombie R E 1997 Near-surface attenuation and site effects from comparison of surface and deep borehole recordings. *Bull. Seismol. Soc. Am.* **87**, 731–744

Abercrombie R E 2000 Crustal attenuation and site effects at Parkfield, California. *J. Geophys. Res.* **105**, 6277–6286

Aki K 1969 Analysis of the seismic coda of local earthquakes as scattered waves. *J. Geophys. Res.* **74**, 615–631

Al-Eqabi G I, Wysession M E 2006 Q_{Lg} distribution in the Basin and Range province of the western United States. *Bull. Seismol. Soc. Am.* **96**, 348–354

Al-Khatib H H, Mitchell B J 1991 Upper mantle anelasticity and tectonic evolution of the western United States from surface wave attenuation. *J. Geophys. Res.* **96**, 18,129–18,146

Al-Shukri H J, Mitchell B J, Ghalib H A A 1988 Attenuation of seismic waves in the New Madrid seismic zone. *Seismol. Res. Lett.* **59**, 133–140

Anderson D L, Given J W 1982 Absorption band Q model for the Earth. *J. Geophys. Res.* **87**, 3893–3904

Anderson D L, Ben-Menahem A, Archambeau C B 1965 Attenuation of seismic energy in the upper mantle. *J. Geophys. Res.* **70**, 1441–1448

Angenheister G H 1906 Bestimmung der fortpflanzungsgeschwindigkeit und absorption von erdbebenwellen, die durch den gegenpunkt des Herdes gegangen sind. *Nachrichten von der Königlichen Gesellschaft der Wissenschaften zu Göttingen* , 110–120

Angenheister G H 1921 Beobachtungen an pazifischen beben. *Nachrichten von der Königlichen Gesellschaft der Wissenschaften zu Göttingen* , 113–146

Artemieva I M, Mooney W D 2001 Thermal thickness and evolution of Precambrian lithosphere: A global study. *J. Geophys. Res.* **106**, 16,387–16,414

Artiemeva I M, Billien M, Lèvêque J J, Mooney D 2004 Shear-wave velocity, seisic attenuation, and thermal structure of the continental upper mantle. *Geophys. J. Int.* **157**, 607–628

Asada T, Takano K 1963 Attenuation of short-period P waves in the mantle. *J. Phys. Earth* **11**, 25–34

Baqer S, Mitchell B J 1998 Regional variation of Lg coda Q in the continental United States and its relation to crustal structure and evolution. *Pure Appl. Geophys.* **153**, 613–638

Benz H M, Frankel A, Boore D M 1997 Regional Lg attenuation for the continental United States. *Bull. Seismol. Soc. Am.* **87**, 606–619

Bollinger G A 1979 Attenuation of the Lg phase and determination of m_b in thee southeastern United States. *Bull. Seismol. Soc. Am.* **69**, 45–63

Bowman J R, Kennett B L N 1991 Propagation of Lg waves in the North Australian craton: Influence of crustal velocity gradients. *Bull. Seismol. Soc. Am.* **81**, 592–610

Brune J N 1970 Tectonic stress and the spectra of seismic shear waves from earthquakes. *J. Geophys. Res.* **75**, 4997–5009

Campillo M, Plantet J L, Bouchon M 1985 Frequency-dependent attenuation in the crust beneath central France from Lg waves: Data analysis and numerical modeling. *Bull. Seismol. Soc. Am.* **75**, 1395–1411

Canas J A, Mitchell B J 1978 Lateral variation of surface-wave anelastic attenuation across the Pacific. *Bull. Seismol. Soc. Am.* **68**, 1637–1650

Canas J A, Mitchell B J 1981 Rayleigh-wave attenuation and its variation across the Atlantic Ocean. *Geophys. J. R. astr. Soc.* **67**, 159–176

Carpenter P J, Sanford A R 1985 Apparent Q for upper crustal rocks of the central Rio Grande Rift. *J. Geophys. Res.* **90**, 8661–8674

Chavez D, Priestley K F 1986 Measurement of frequency dependent Lg attenuation in the Great Basin. *Geophys. Res. Lett.* **60**, 551–554

Chen P F, Bina C R, Okal E A 2001 Variations in slab dip along the subducting Nazca plate, as related to stress patterns and moment release of intermediate-depth seismicity and to surface volcanism. *Geochem. Geophys. Geosyst.* **2**, 2001GC000,153

Cheng C C, Mitchell B J 1981 Crustal Q structure in the United States from multi-mode surface waves. *Bull. Seismol. Soc. Am.* **71**, 161–181

Chouet B 1979 Temporal varation in the attenuation of earthquake coda near Stone Canyon, California. *Geophys. Res. Lett.* **6**, 143–146

Chun K Y, West G F, Kikoski R J, Samson C 1987 A novel technique for measuring Lg attenuation - Results from eastern Canada between 1-Hz and 10-Hz. *Bull. Seismol. Soc. Am.* **77**, 398–419

Cong L, Mitchell B J 1998 Seismic velocity and Q structure of the Middle Eastern crust and upper mantle from surface-wave dispsersion and attenuation. *Pure Appl. Geophys.* **153**, 503–538

Dainty A M 1981 A scattering model to explain Q observations in the lithosphere between 1 and 30 Hz. *Geophys. Res. Lett.* **8**, 1126–1128

Davies J H 1999 The role of hydraulic fractures and intermediate-depth earthquakes in generating subduction-zone magmatism. *Nature* **398**, 142–145

DeSouza J L, Mitchell B J 1998 Lg coda Q variations across South America and their relation to crustal evolution. *Pure Appl. Geophys.* **153**, 587–612

Eberhart-Phillips D, Chadwick M 2002 Three-dimensional attenuation model of the shallow Hikurangi subduction zone in the Raukumara Peninsula, New Zealand. *J. Geophys. Res.* **107**, 2033, doi:10.1029/2000JB000,046

Ekström G, Tromp J, Larson E W F 1997 Measurements and global models of surface wave propagation. *J. Geophys. Res.* **102**, 8137–8157

Evernden J F 1955 Tripartite results for the Kamchatka earthquake of November 4, 1952. *Bull. Seismol. Soc. Am.* **45**, 167–178

Frankel A, Wennerberg L 1987 Energy-flux model for seismic coda: Separation of scattering and intrinsic attenuation. *Bull. Seismol. Soc. Am.* **77**, 1223–1251

Futterman W I 1962 Dispersive body waves. *J. Geophys. Res.* **67**, 5279–5291

Gutenberg B 1924 Dispersion und extinktion von seismischen oberflächenwellen und der aufbau der obersten erdschichten. *Phys. Zeitschr.* **25**, 377–381

Gutenberg B 1945a Amplitudes of surface waves and magnitudes of shallow earthquakes. *Bull. Seismol. Soc. Am.* **35**, 3–12

Gutenberg B 1945b Amplitudes of P, PP, and S and magnitude of shallow earthquakes. *Bull. Seismol. Soc. Am.* **35**, 57–69

Gutenberg B 1958 Attenuation of seismic waves in the Earth's mantle. *Bull. Seismol. Soc. Am.* **48**, 269–282

Hasegawa H S 1974 Theoretical synthesis and analysis of strong motion spectra of earthquakes. *Can. Geotech. J.* **11**, 278–297

Hasegawa H S 1985 Attenuation of Lg waves in the Canadian shield. *Bull. Seismol. Soc. Am.* **75**, 1569–1582

Hauksson E, Shearer P M 2006 Attenuation models (Q_P and Q_S) in three dimensions of the southern California crust: Inferred fluid saturation at seismogenic depths. *J. Geophys. Res.* **111**, B05,302, doi:10.1029/2005JB003,947

Herrmann R B 1980 Q estimates using the coda of local earthquakes. *Bull. Seismol. Soc. Am.* **70**, 447–468

Herrmann R B, Mitchell B J 1975 Statistical analysis and interpretation of surface-wave anelastic attenuation data for the stable interior of North America. *Bull. Seismol. Soc. Am.* **65**, 1115–1128

Hoshiba M 1991 Simulation of multiple-scattering coda wave excitation based on the energy conservation law. *Phys. Earth Planet. Inter.* **67**, 123–136

Hough S E, Anderson J G, Brune J, Vernon III F, Berger J, Fletcher J, Haar L, Hanks T, Baker L 1988 Attenuation near Anza, California. *Bull. Seismol. Soc. Am.* **78**, 672–691

Hough S E, Lees J M, Monastero F 1999 Attenuation and source properties at the Coso geothermal area, California. *Bull. Seismol. Soc. Am.* **89**, 1606–1619

Humphreys E, Clayton R W 1988 Adaptation of back projection tomography to seismic travel time problems. *J. Geophys. Res.* **93**, 1073–1086

Hwang H J, Mitchell B J 1987 Shear velocities, Q_β, and the frequency dependence of Q_β in stable and tectonically active regions from surface wave observations. *Geophys. J. R. astr. Soc.* **90**, 575–613

Ichikawa M, Basham P W 1965 Variations in short-period records from Canadian seismograph statons. *Can. J. Earth Sci.* **2**, 510–542

Jeffreys H 1967 Radius of the Earth's core. *Nature* **215**, 1365–1366

Jemberie A L, Mitchell B J 2004 Shear-wave Q structure and its lateral variation in the crust of China and surrounding regions. *Geophys. J. Int.* **157**, 363–380

Jin A, Aki K 1986 Temporal change in coda Q before the Tangshan earthquake of 1976 and the Haicheng earthquake of 1975. *J. Geophys. Res.* **91**, 665–673

Kijko A, Mitchell B J 1983 Multimode Rayleigh wave attenuation and Q_β in the crust of the Barents shelf. *J. Geophys. Res.* **88**, 3315–3328

Knopoff L 1964 Q. *Rev. Geophys.* **2**, 625–660

Liu H P, Anderson D L, Kanamori H 1976 Velocity dispersion due to anelasticity: Implications for seismology and mantle composition. *Geophys. J. R. astr. Soc.* **47**, 41–58

Lomnitz C 1957 Linear dissipation in solids. *J. Applied Phys.* **28**, 201–205

Malin P E 1978 *A first order scattering solution for modeling lunar and terrestrial seismic coda.* Ph.d. dissertation, Princeton Univ., Princeton, NJ

Mitchell B J 1973 Radiation and attenuation of Rayleigh waves from the southeastern Missouri earthquake of October 21, 1965. *J. Geophys. Res.* **78**, 886–899

Mitchell B J 1975 Regional Rayleigh wave attenuation on North America. *J. Geophys. Res.* **35**, 4904–4916

Mitchell B J 1995 Anelastic structure and evolution of the continental crust and upper mantle from seismic surface wave attenuation. *Rev. Geophys.* **33**, 441–462

Mitchell B J, Cong L 1998 *Lg* coda Q and its relation to the structure and evolution of continents: A global perspective. *Pure Appl. Geophys.* **153**, 655–663

Mitchell B J, Hwang H J 1987 The effect of low-Q sediments and crustal Q on *Lg* attenuation in the United States. *Bull. Seismol. Soc. Am.* **77**, 1197–1210

Mitchell B J, Xie J 1994 Attenuation of multiphase surface waves in the Basin and Range province, III, Inversion for crustal anelasticity. *Geophys. J. Int.* **116**, 468–484

Mitchell B J, Pan Y, Xie J, Cong L 1997 *Lg* coda Q across Eurasia and its relation to crustal evolution. *J. Geophys. Res.* **102**, 22,767–22,779

Mitchell B J, Baqer S, Akinci A, Cong L 1998 *Lg* coda Q in Australia and its relation to crustal structure and evolution. *Pure Appl. Geophys.* **153**, 639–653

Mitchell B J, Cong L, Ekström G 2006 A continent-wide 1-Hz map of *Lg* coda Q variation across Eurasia and its implications for crustal evolution. *J. Geophys. Res.* , submitted

Modiano T, Hatzfeld D 1982 Experimental study of the spectral content for shallow earthquakes. *Bull. Seismol. Soc. Am.* **72**, 1739–1758

Nuttli O W 1973 Seismic wave attenuation and magnitude relations for eastern North America. *J. Geophys. Res.* **78**, 876–885

Nuttli O W 1978 A time-domain study of the attenuation of 10-Hz waves in the New Madrid seismic zone. *Bull. Seismol. Soc. Am.* **68**, 343–355

Nuttli O W 1980 The excitation and attenuation of seismic crustal phases in Iran. *Bull. Seismol. Soc. Am.* **70**, 469–484

O'Connell R J, Budiansky B 1978 Measures of dissipation in viscoelastic media. *Geophys. Res. Lett.* **5**, 5–8

Ojeda A, Ottemöller L 2002 Q_{Lg} tomography in Colombia. *Phys. Earth Planet. Inter.* **130**, 253–270

Ottemöller L, Shapiro N M, Singh S K, Pacheco J F 2002 Lateral variation of *Lg* wave propagation in southern Mexico. *J. Geophys. Res.* **107**, B1,2008,10.1029/2001JB000,206

Patton H J, Taylor S R 1989 Q structure of the Basin and Range from surface waves. *J. Geophys. Res.* **89**, 6929–6940

Press F 1956 Rigidity of the Earth's core. *Science* **124**, 1204

Richards P G, Menke W 1983 The apparent attenuation of a scattering medium. *Bull. Seismol. Soc. Am.* **73**, 1005–1021

Sarker G, Abers G A 1998 Comparison of seismic body wave and coda wave measures of Q. *Pure Appl. Geophys.* **153**, 665–683

Schlotterbeck B A, Abers G A 2001 Three-dimensional attenuation variations in southern California. *J. Geophys. Res.* **106**, 30,719–30,735

Shearer P M 2006 Seismic scattering in the deep Earth. *Treatise on Geophysics* , in press

Shi J, Kim W Y, Richards P G 1996 Variability of crustal attenuation in the northeastern United States from *Lg* waves. *J. Geophys. Res.* **101**, 25,231–25,242

Singh S, Herrmann R B 1983 Regionalization of crustal Q in the continental United States. *J. Geophys. Res.* **88**, 527–538

Street R L 1976 Scaling northeastern United States/southeastern Canadian earthquakes by the *Lg* waves. *Bull. Seismol. Soc. Am.* **66**, 1525–1537

Strick E 1967 The determination of Q, dynamic viscosity and creep curves from wave propagation measurements. *Geophys. J. R. astr. Soc.* **13**, 197–218

Sutton G H, Mitronovas W, Pomeroy P W 1967 Short-period seismic energy radiation patterns from underground explosions and small-magnitude earthquakes. *Bull. Seismol. Soc. Am.* **57**, 249–267

Thouvenot F 1983 Frequency dependence of the quality factor in the upper crust: A deep seismic sounding approach. *Geophys. J. R. astr. Soc.* **73**, 427–447

Tryggvason E 1965 Dissipation of Rayleigh-wave energy. *J. Geophys. Res.* **70**, 1449–1455

Tsai Y B, Aki K 1969 Simultaneous determination of the seismic moment and attenuation of seismic surface waves. *Bull. Seismol. Soc. Am.* **59**, 275–287

Utsu T 1967 Anomalies in seismic wave velocity and attenuation associated with a deep earthquake zone. *J. Fac. Sci., Hokkaido Univ.* **7**, 1–25

Wilcock W S D, Solomon S C, Purdy G M, Toomey D R 1995 Seismic attenuation structure of the East Pacific Rise near 9° 30m N. *J. Geophys. Res.* **100**, 24,147–24,165

Xie J, Mitchell B J 1990a A back-projection method for imaging large-scale lateral variations of *Lg* coda Q with application to continental Africa. *Geophys. J. Int.* **100**, 161–181

Xie J, Mitchell B J 1990b Attenuation of multiphase surface waves in the Basin and Range province, I. *Lg* and *Lg* coda. *Geophys. J. Int.* **102**, 121–127

Xie J, Nuttli O W 1988 Interpretation of high-frequency coda at large distances: Stochastic modeling and method of inversion. *Geophys. J.* **95**, 579–595

Xie J, Gok R, Ni J, Aoki Y 2004 Lateral variations of crustal seismic attenuation along the INDEPTH profiles in Tibet from *LgQ* inversion. *J. Geophys. Res.* **109**, B10,308, doi:10.1029/2004JB002,988

Xie J, Wu X, Liu R, Schaff D, Liu Y, Liang J 2006 Tomographic regionalization of crustal *Lg Q* in eastern Eurasia. *Geophys. Res. Lett.* **33**, L03,315, doi:10.1029/2005GL024,410

Yacoub N K, Mitchell B J 1977 Attenuation of Rayleigh wave amplitudes across Eurasia. *Bull. Seismol. Soc. Am.* **67**, 751–769

Zeng Y 1991 Compact solutions for multiple scattered wave energy in time domain. *Bull. Seismol. Soc. Am.* **81**, 1022–1029

Zeng Y, Su F, Aki K 1991 Scattered wave energy propagation in a random isotropic scattering medium. *J. Geophys. Res.* **96**, 607–619

Zhang T, Lay T 1994 Analysis of short-period regional phase path effects associated with topography in Eurasia. *Bull. Seismol. Soc. Am.* **84**, 119–132

Figure 1. (a) Internal friction (Q^{-1}), (b) phase and group velocity dispersion, and (c) attenuation coefficient as functions of frequency. From Liu et al. (1976).

Figure 2. Seismograms recorded at stations CCM (Cathedral Cave, MO) and PAS (Pasadena, CA) for the mb4.5 event in southeastern New Mexico that occurred on January 2, 1992 at 11:45:35.6 UT. The epicentral distance to CCM (along a relatively high-Q path) is 1256 km and to PAS (along a relatively low-Q path) is 1417 km. From Mitchell (1995).

Figure 3. Left - Three Q_μ models resulting from the inversion of Rayleigh-wave attenuation coefficient data from the Basin and Range province. The numbers refer to the values of Q_o and η predicted by the three models for Q_{Lg}. Right - Three selected models for the variation of Q_μ frequency dependence with depth in the crust of the Basin and Range province. Each of these depth distributions was fixed during inversions that produced the Q_μ models.

Figure 4. Seismograms and SSR's for a relatively high-Q (701) path to station HYB in India, a relatively low-Q (359) path to station BJT in northern China and a low-Q path (208) path to station LSA in Tibet. From Mitchell et al. (2006).

Figure 5. (a) A scattering ellipse map, (b) a Q_o map, and (c) an η map for Eurasia. Adapted from Mitchell et al. (1997).

Figure 6. Simplified tectonic map of Eurasia from Mitchell et al. (1997).

Figure 7. Q_μ maps for China and peripheral regions for (left) the depth range 0-10 km, (right) the depth range 10-30 km. Adapted from Jemberie and Mitchell (2004).

Figure 8. (a) A scattering ellipse map, (b) a Q_o map, and (c) an η map for Africa. Adapted from Xie and Mitchell (1990b).

Figure 9. (a) A scattering ellipse map, (b) a Q_o map, and (c) an η map for South America. Adapted from DeSouza and Mitchell (1998).

Figure 10. (a) A scattering ellipse map, (b) a Q_o map and (c) an *eta* map of Q_{Lg}^C for Australia. Adapted from Mitchell et al. (1998).

Figure 11. (a) A scattering elipse map, (b) a Q_o map and (c) an *eta* map of Q_{Lg}^C for the United States. Adapted from Baqer and Mitchell (1998).

Figure 12. Results of inversion for along-axis variations in the upper crust of the East Pacific Rise and peripheral regions near $90^o30'$ N latitude. (a) The axisymmetric starting model obtained from a two-dimensional inversion of t^* values for upper crustal wave paths, (b) A vertical cross-section through the three-dimensional solution aligned along the rise axis, and (c) A horizontal cross-section at 2.75 km depth. Numbers on the cross-sectons and map denote values of Q_{-1} for P waves. From Wilcock et al. (1995).

Figure 13. Q_o for Q_{Lg}^C at 1 Hz versus time elapsed in selected regions since the most recent episode of tectonic or orogenic activity.

Fig. 1

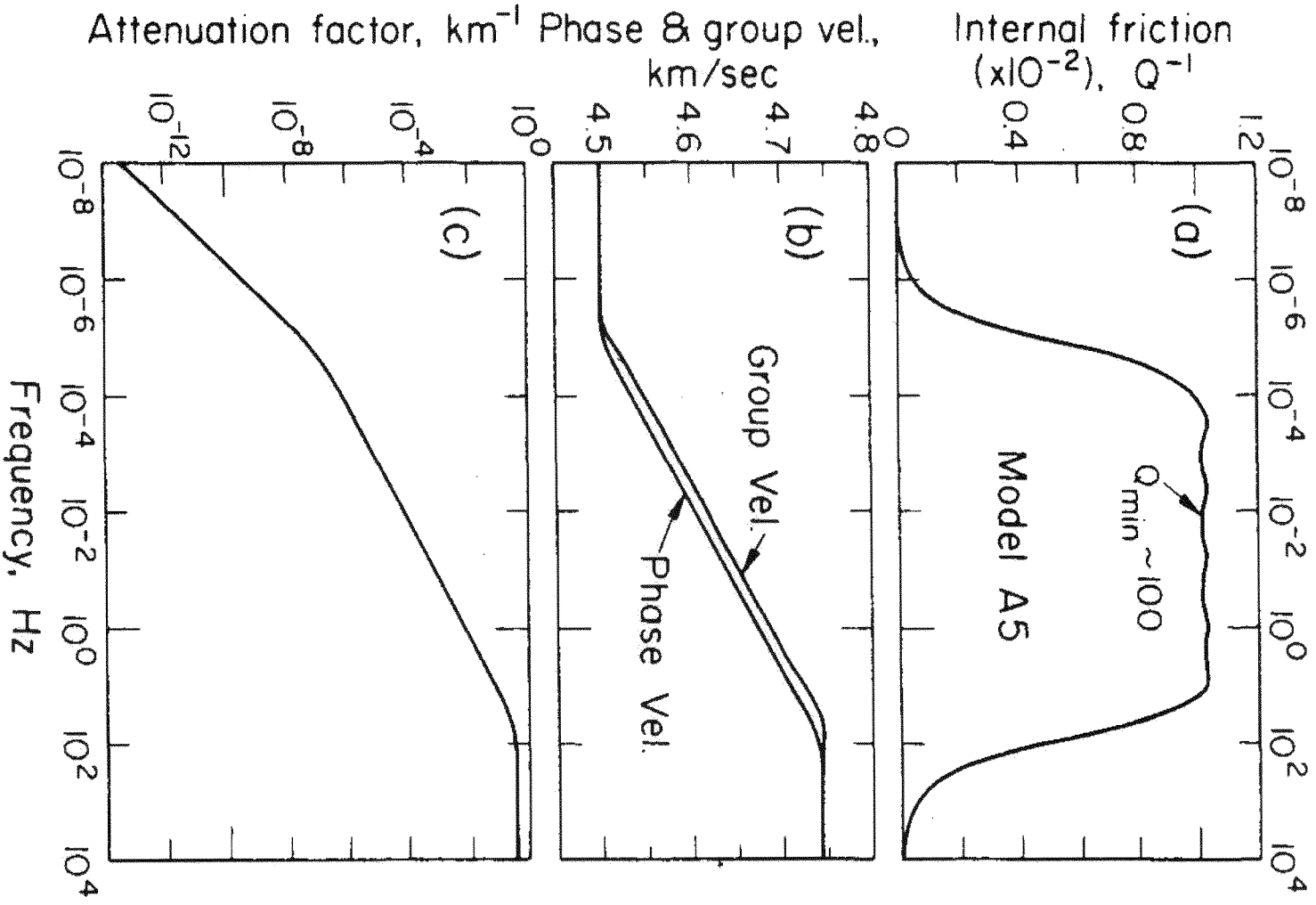
Internal friction
(x10⁻²), Q⁻¹
0
0.4
0.8
1.2
(a)
Model A5
Q_min ~ 100
10⁻⁸
10⁻⁶
10⁻⁴
10⁻²
10⁰
10²
10⁴
Phase & group vel.,
km/sec
4.5
4.6
4.7
4.8
(b)
Group Vel.
Phase Vel.
Attenuation factor, km⁻¹
10⁻¹²
10⁻⁸
10⁻⁴
10⁰
(c)
Frequency, Hz

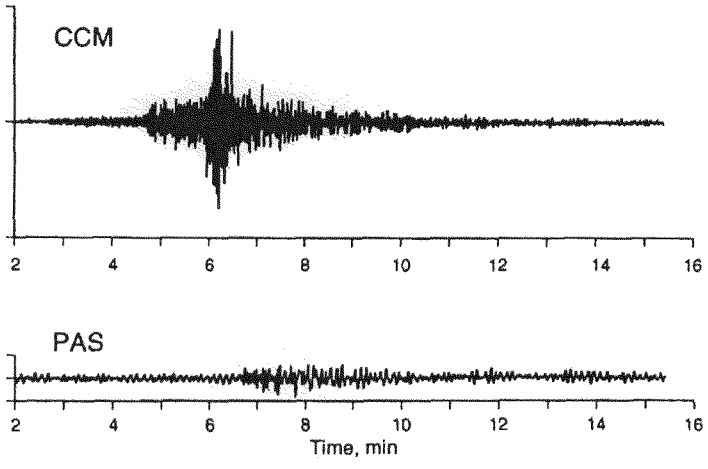

Fig. 2

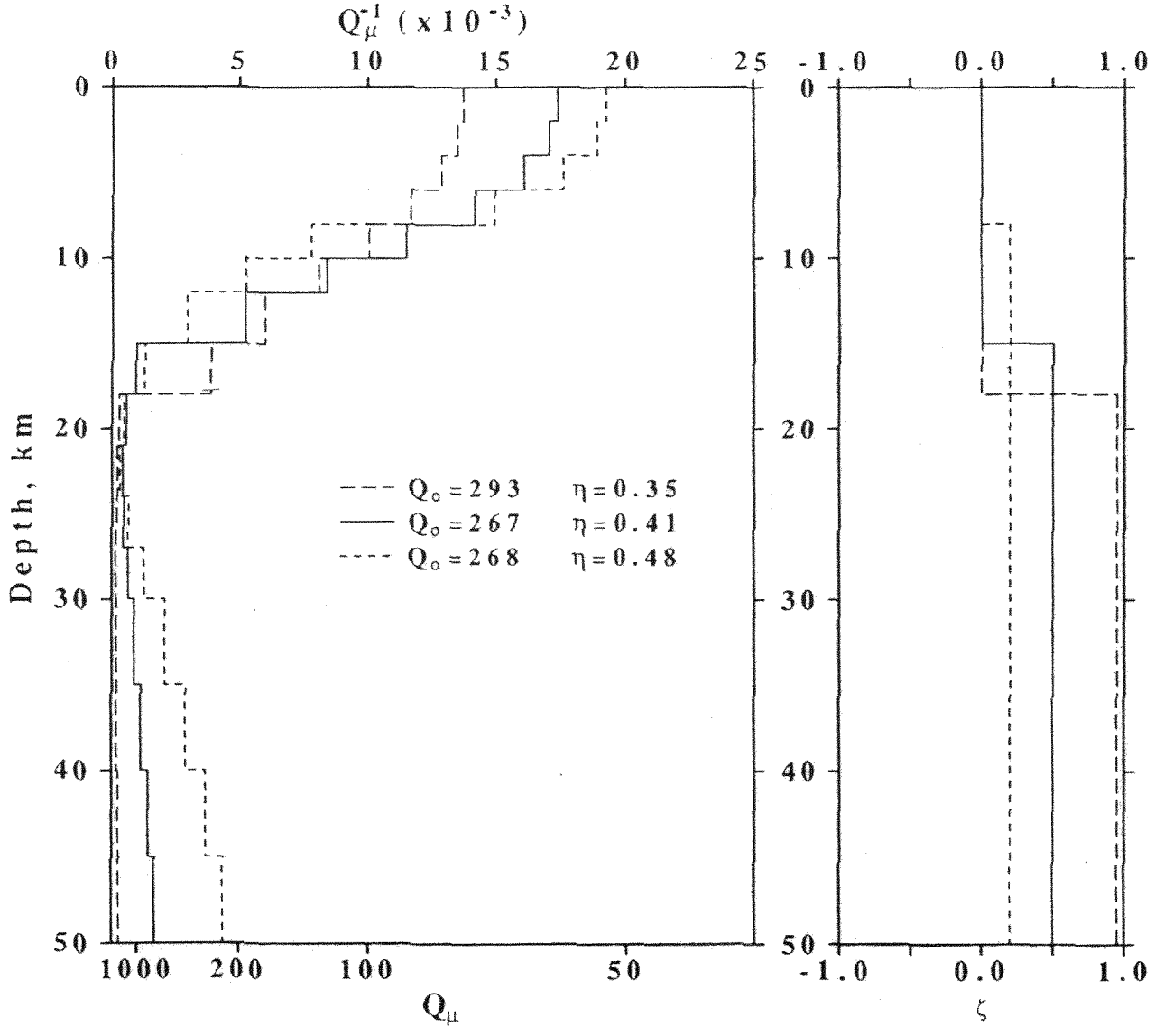
Q_μ^{-1} (x 10 $^{-3}$)
0
5
10
15
20
25
-1.0
0.0
1.0
Depth, km
0
10
20
30
40
50
Q_o = 293 η = 0.35
Q_o = 267 η = 0.41
Q_o = 268 η = 0.48
1000
200
100
50
Q_μ
ζ

Fig. 3

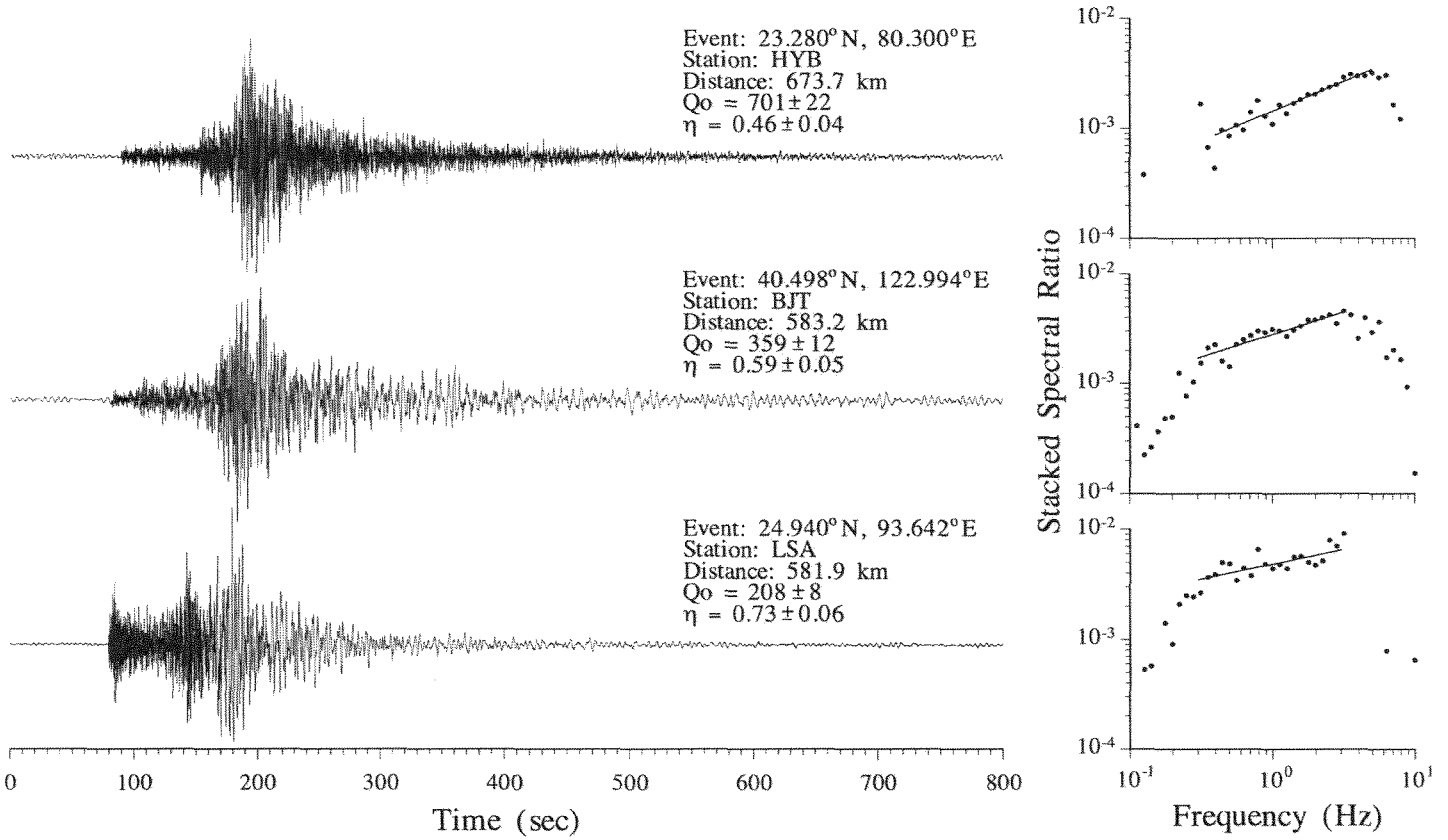
Event: 23.280°N, 80.300°E
Station: HYB
Distance: 673.7 km
Qo = 701±22
η = 0.46±0.04
Event: 40.498°N, 122.994°E
Station: BJT
Distance: 583.2 km
Qo = 359±12
η = 0.59±0.05
Event: 24.940°N, 93.642°E
Station: LSA
Distance: 581.9 km
Qo = 208±8
η = 0.73±0.06
0
100
200
300
400
500
600
700
800
Time (sec)
Stacked Spectral Ratio
10^{-2}
10^{-3}
10^{-4}
10^{-1}
10^{0}
10^{1}
Frequency (Hz)

Fig. 4

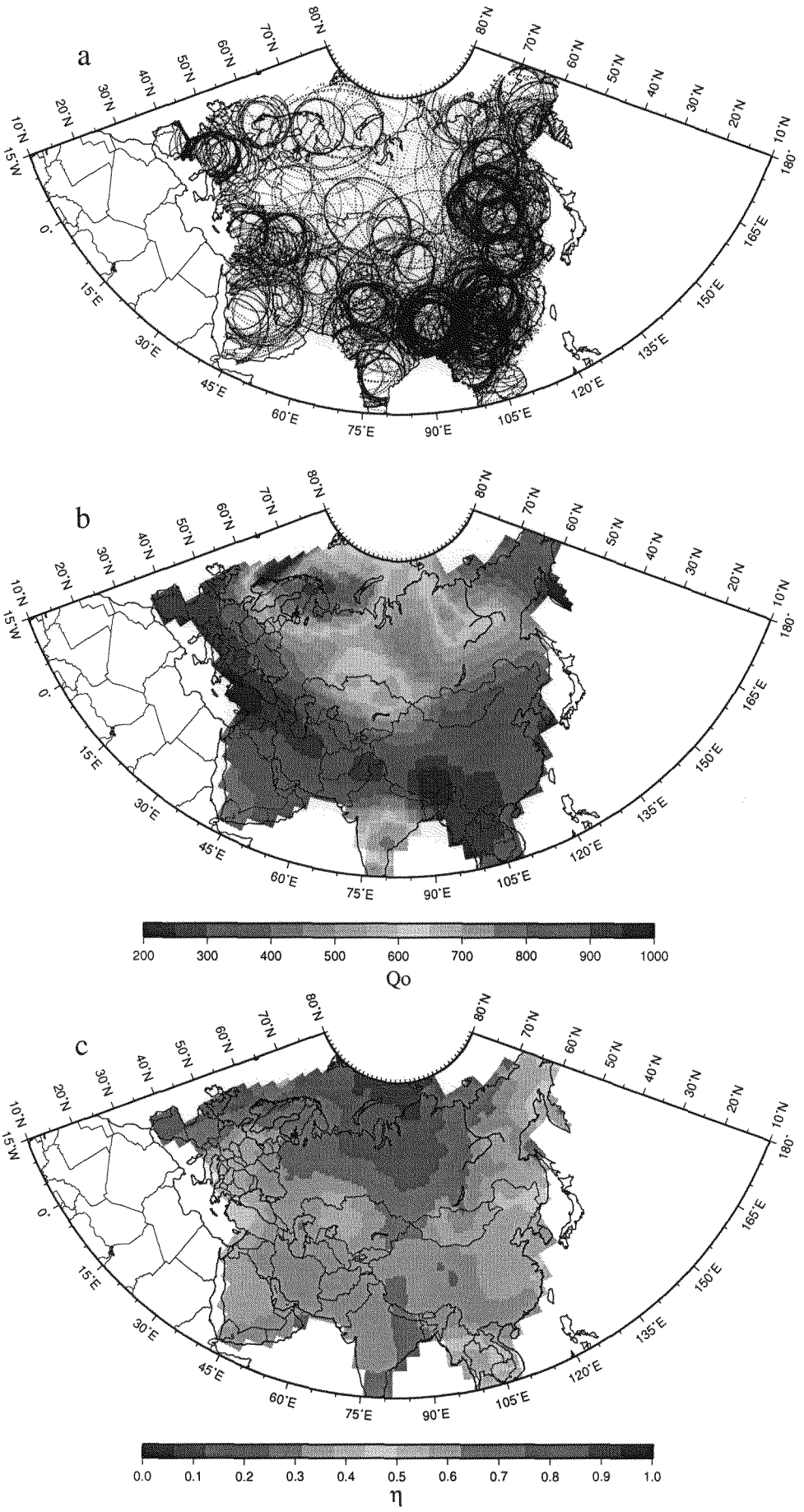
a
b
c
80°N
70°N
60°N
50°N
40°N
30°N
20°N
10°N
15°W
0°
15°E
30°E
45°E
60°E
75°E
90°E
105°E
120°E
135°E
150°E
165°E
180°
200
300
400
500
600
700
800
900
1000
Qo
0.0
0.1
0.2
0.3
0.4
0.5
0.6
0.7
0.8
0.9
1.0
η

Fig 5

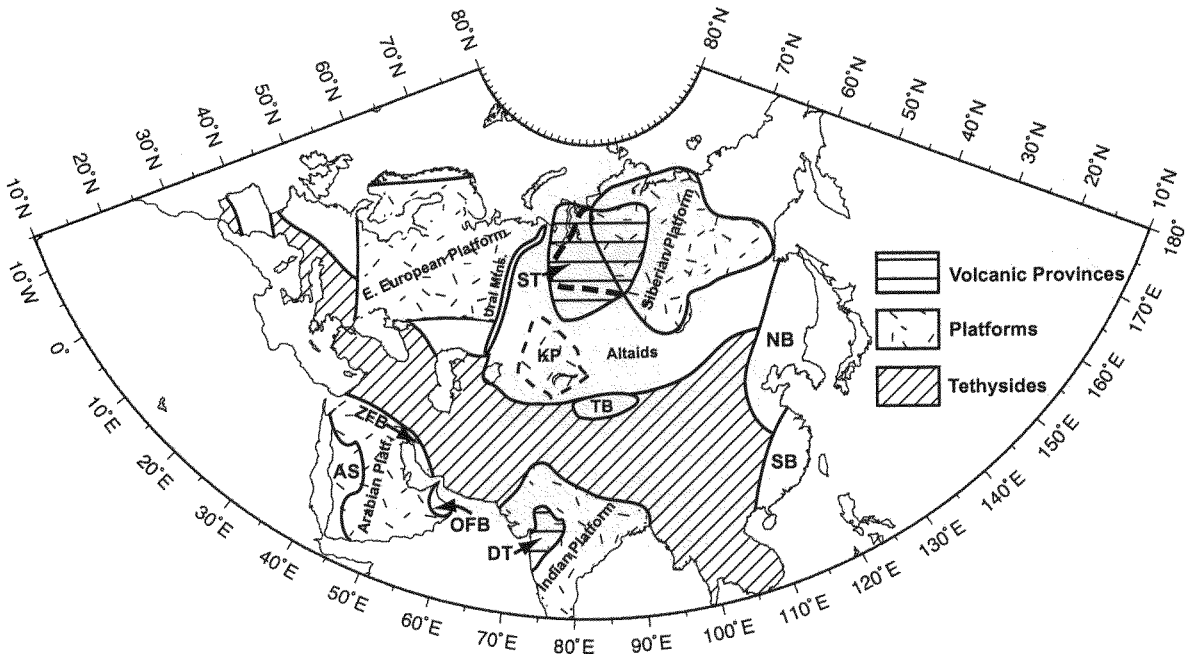
Volcanic Provinces
Platforms
Tethysides
E. European Platform
Ural Mtns.
Siberian Platform
ST
KP
Altaids
NB
TB
SB
ZEB
AS
Arabian Platf.
OFB
DT
Indian Platform
80°N
70°N
60°N
50°N
40°N
30°N
20°N
10°N
10°W
0°
10°E
20°E
30°E
40°E
50°E
60°E
70°E
80°E
90°E
100°E
110°E
120°E
130°E
140°E
150°E
160°E
170°E
180°

Fig. 6

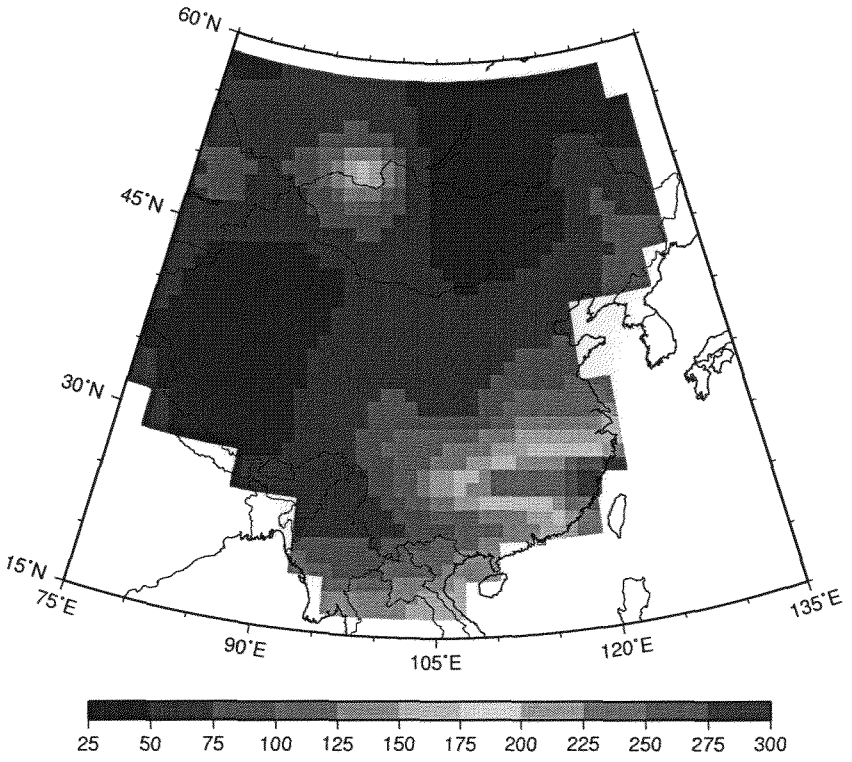

Q_μ - 0 to 10 km depth

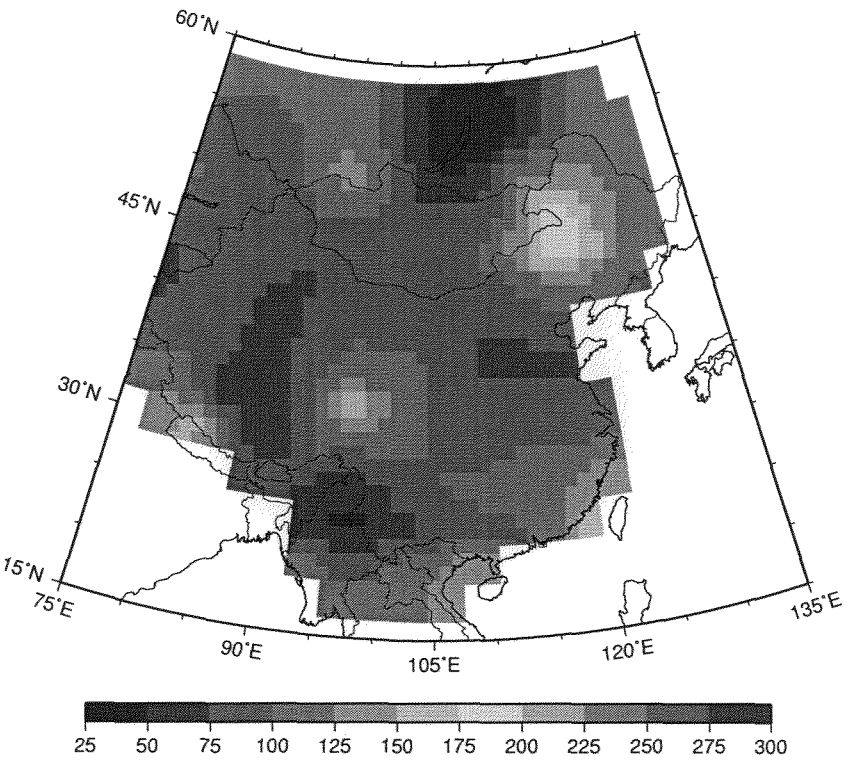

Q_μ - 10 to 30 km depth

Fig. 7

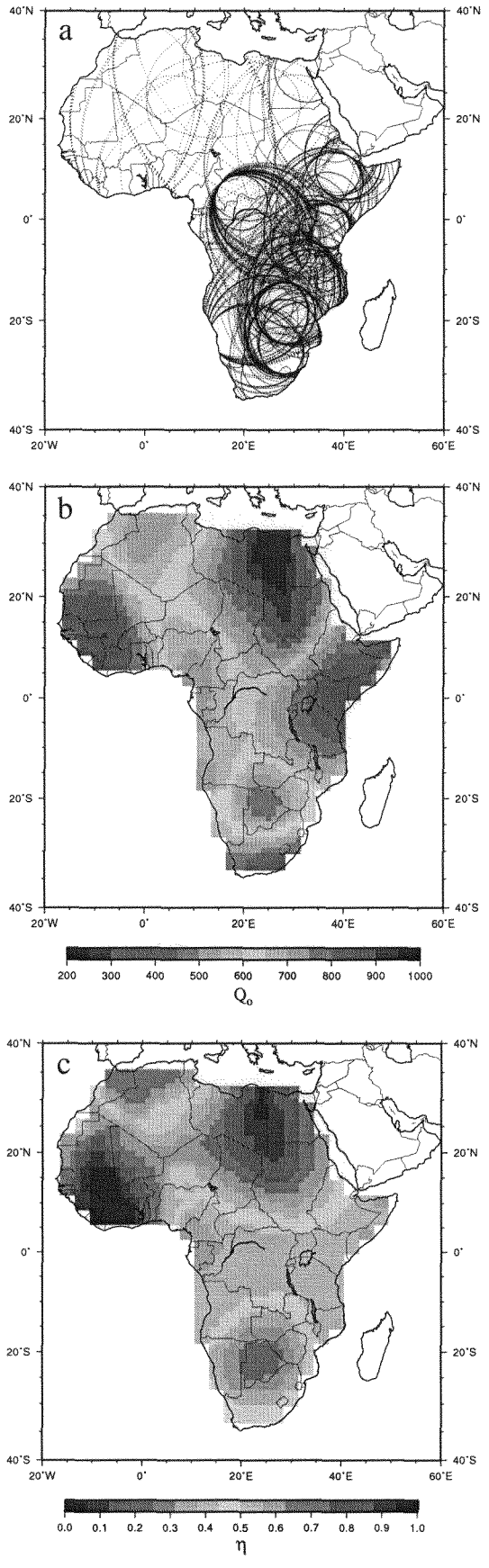
a
b
c
40°N
20°N
0°
20°S
40°S
20°W
0°
20°E
40°E
60°E
200 300 400 500 600 700 800 900 1000
Q_o
0.0 0.1 0.2 0.3 0.4 0.5 0.6 0.7 0.8 0.9 1.0
η

Fig. 8

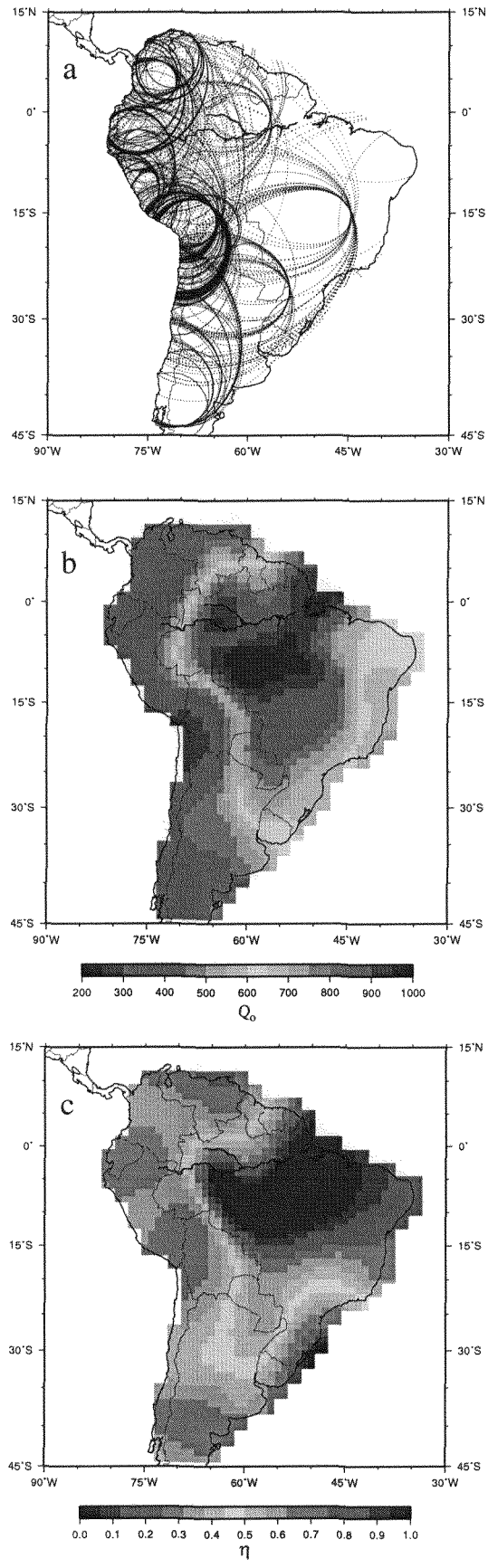
a
b
c
15°N
0°
15°S
30°S
45°S
90°W
75°W
60°W
45°W
30°W
200 300 400 500 600 700 800 900 1000
Q_o
0.0 0.1 0.2 0.3 0.4 0.5 0.6 0.7 0.8 0.9 1.0
η

Fig. 9

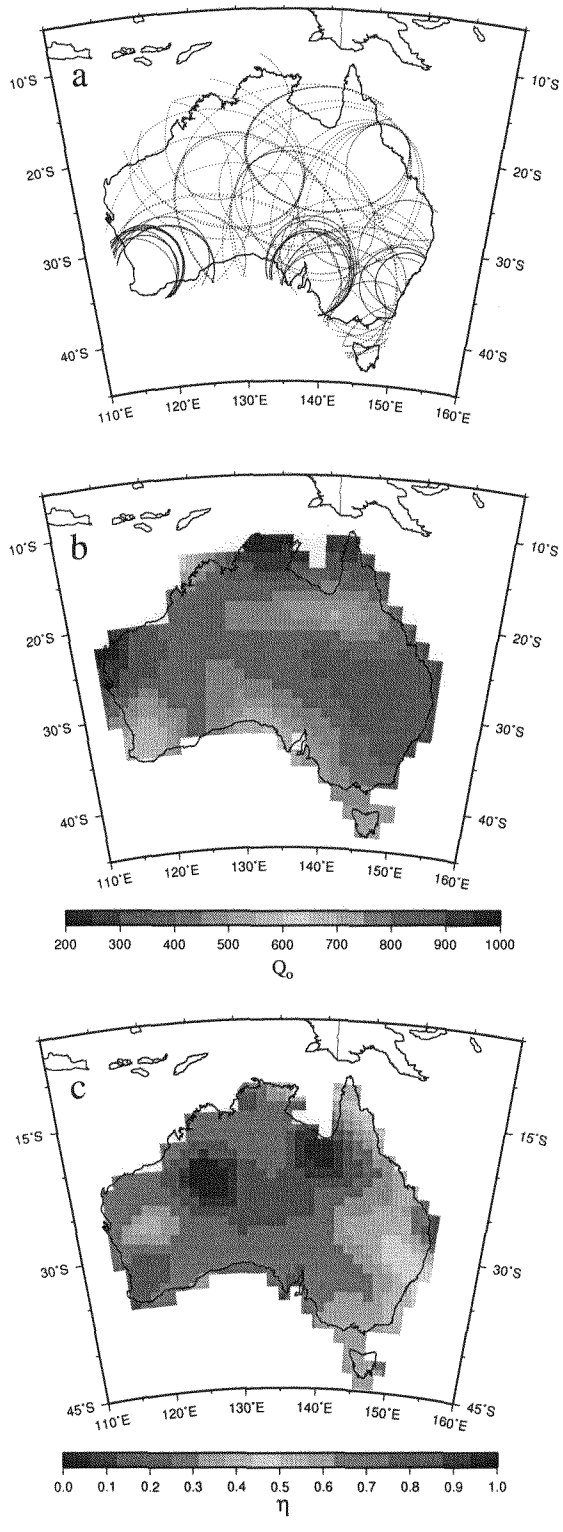
a
10°S
20°S
30°S
40°S
110°E
120°E
130°E
140°E
150°E
160°E
b
200
300
400
500
600
700
800
900
1000
Q_o
c
15°S
45°S
0.0
0.1
0.2
0.3
0.4
0.5
0.6
0.7
0.8
0.9
1.0
η

Fig. 10

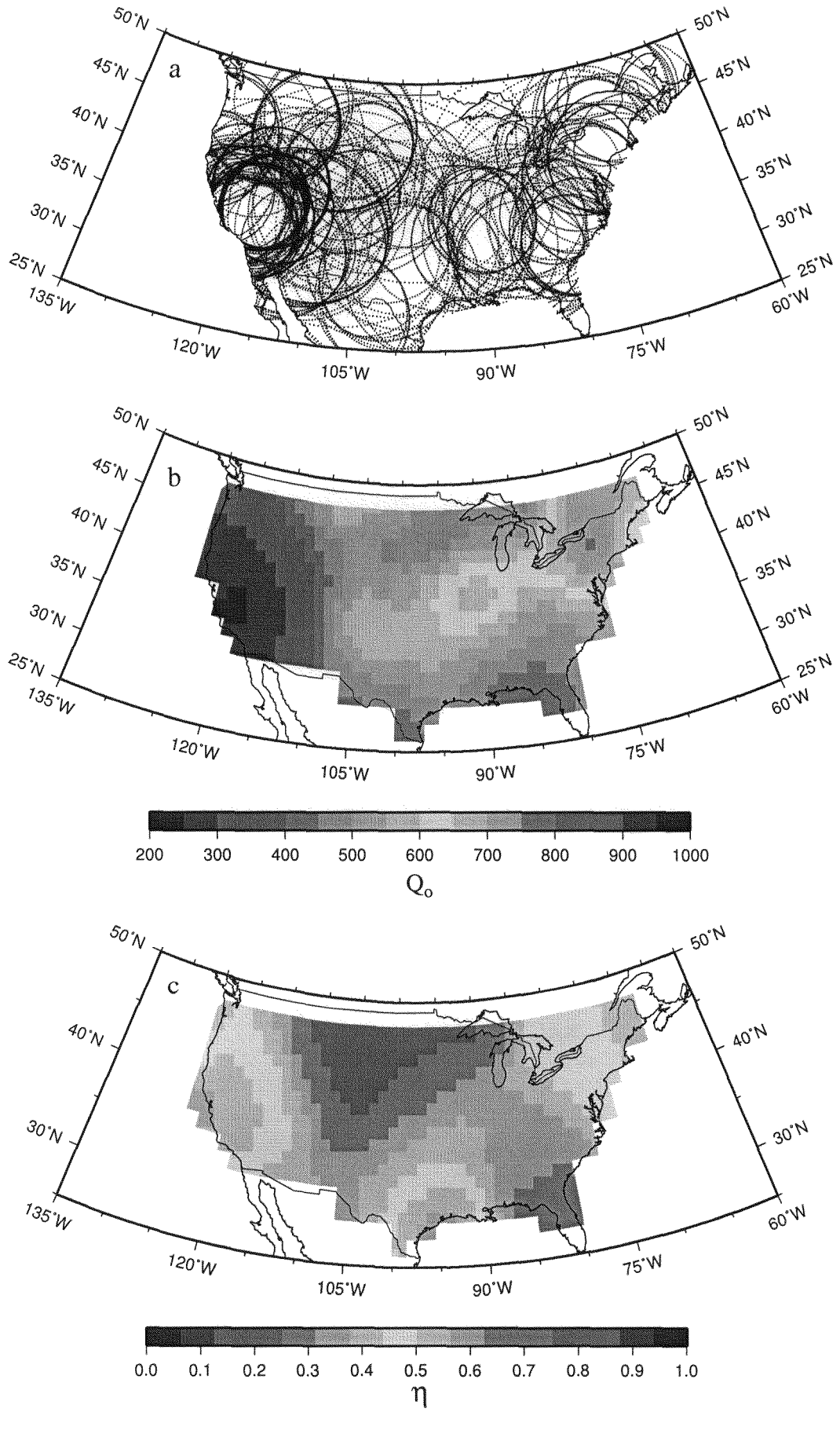
a
b
c
50°N
45°N
40°N
35°N
30°N
25°N
135°W
120°W
105°W
90°W
75°W
60°W
200
300
400
500
600
700
800
900
1000
Q_o
0.0
0.1
0.2
0.3
0.4
0.5
0.6
0.7
0.8
0.9
1.0
η

Fig. 11

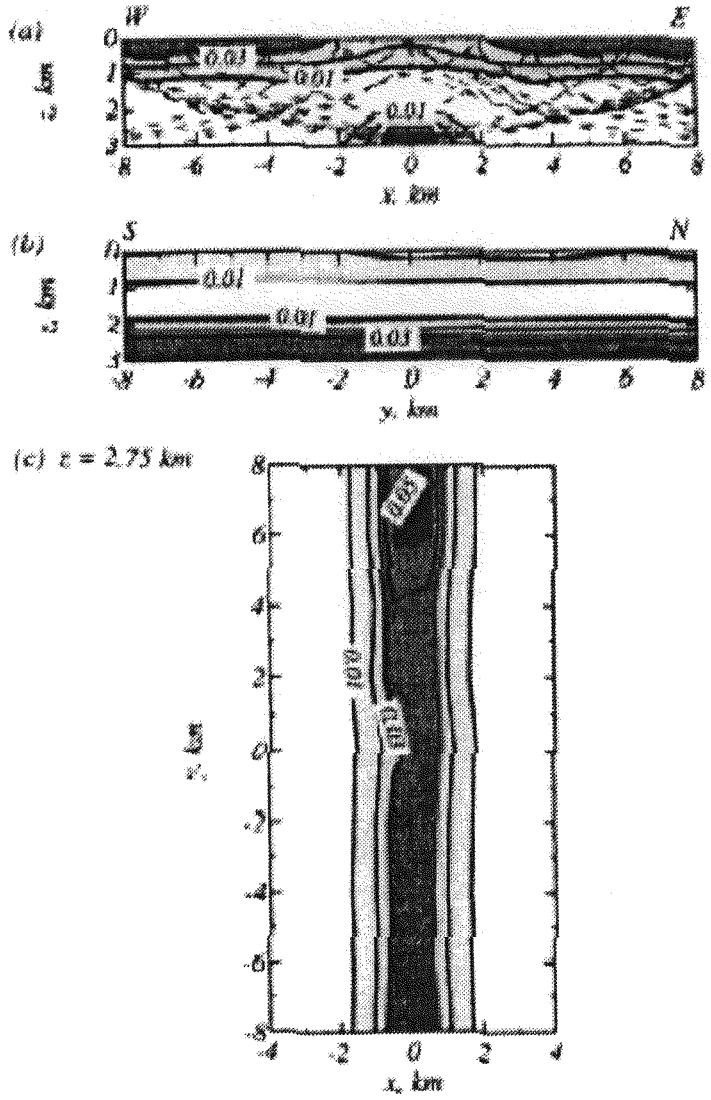
(a)
W
E
0.03
0.01
0.01
z, km
x, km
(b)
S
N
0.01
0.01
0.03
z, km
y, km
(c) z = 2.75 km
0.03
0.02
0.01
y, km
x, km

Fig. 12

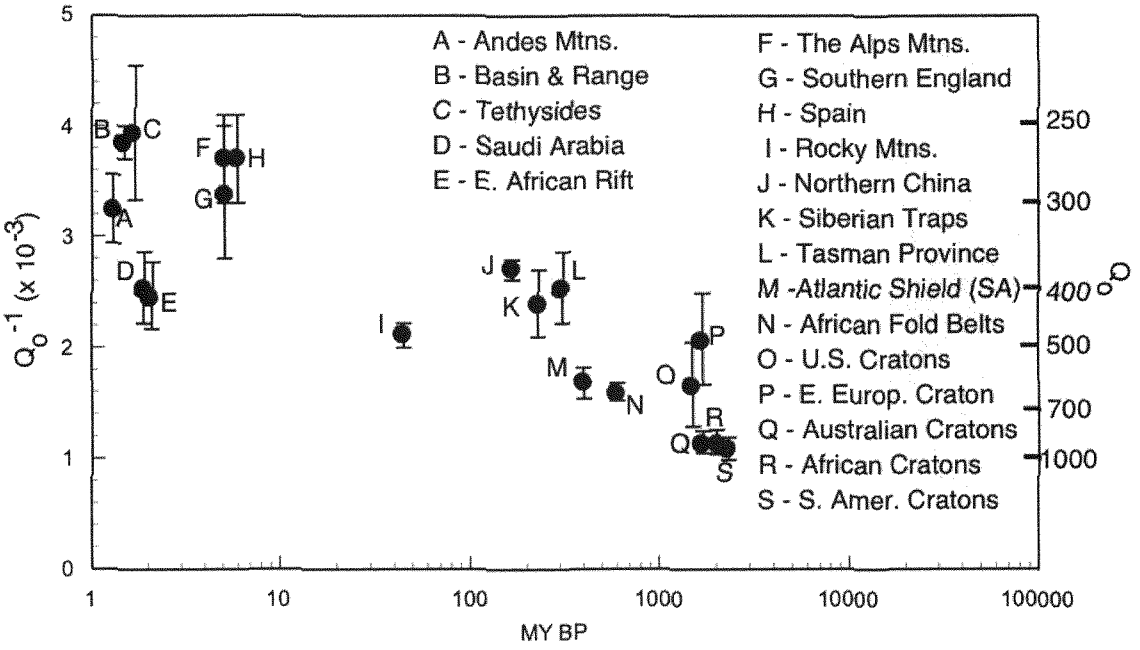
A - Andes Mtns.
B - Basin & Range
C - Tethysides
D - Saudi Arabia
E - E. African Rift
F - The Alps Mtns.
G - Southern England
H - Spain
I - Rocky Mtns.
J - Northern China
K - Siberian Traps
L - Tasman Province
M -Atlantic Shield (SA)
N - African Fold Belts
O - U.S. Cratons
P - E. Europ. Craton
Q - Australian Cratons
R - African Cratons
S - S. Amer. Cratons
Q_o^{-1} (x 10^{-3})
MY BP
Q_o
0
1
2
3
4
5
1
10
100
1000
10000
100000
250
300
400
500
700
1000

Fig. 13